

May 2018

Time-Resolved Structural Enzymology at X-ray Free Electron Lasers

Tyler Norwood

University of Wisconsin-Milwaukee

Follow this and additional works at: <https://dc.uwm.edu/etd>

 Part of the [Biophysics Commons](#), and the [Physics Commons](#)

Recommended Citation

Norwood, Tyler, "Time-Resolved Structural Enzymology at X-ray Free Electron Lasers" (2018). *Theses and Dissertations*. 1886.
<https://dc.uwm.edu/etd/1886>

This Thesis is brought to you for free and open access by UWM Digital Commons. It has been accepted for inclusion in Theses and Dissertations by an authorized administrator of UWM Digital Commons. For more information, please contact open-access@uwm.edu.

TIME-RESOLVED STRUCTURAL ENZYMOLOGY AT X-RAY FREE ELECTRON LASERS

by

Tyler Norwood

A Thesis Submitted in

Partial Fulfillment of the

Requirements for the Degree of

Master of Science

in Physics

at

The University of Wisconsin-Milwaukee

May 2018

ABSTRACT

TIME-RESOLVED STRUCTURAL ENZYMOLOGY AT X-RAY FREE ELECTRON LASERS

by

Tyler Norwood

The University of Wisconsin-Milwaukee, 2018
Under the Supervision of Professor Marius Schmidt

Within the last decade, X-ray Free Electron Lasers (XFELs) have emerged across the world. These XFELs produce X-ray pulses with a duration on the order of femtoseconds, each of which contains 10^{12} photons. Before the XFEL, the brightest X-ray sources were 3rd generation synchrotrons. While these facilities are still very important for many experiments, XFELs allow for time-resolved experiments with femtosecond time resolution and mixing experiments that are not possible at the synchrotron. Enzymatic processes have promising prospects for medicine which use proteins as drug targets and enhance our understanding of these important biomolecules.

A number of procedures are involved alongside an XFEL experiment. Before an experiment, characterization tests should be performed to confirm that the experiment will work on the beamline. Confirmation that crystals diffract can be obtained using an X-ray source either in one's own lab or at a synchrotron. Spectroscopic tests can confirm the initiation of a reaction in a sample and identify the timings of such reactions. In addition to assisting at XFEL experiments, I performed tests such as these to ensure that our group was prepared. After an experiment, the data must be processed before structures can be obtained. Due to the serial nature of XFEL experiments, a program is necessary to detect which images contain Bragg

diffraction. I developed a similar program to perform the same function on serial data collected at a synchrotron.

TABLE OF CONTENTS

ABSTRACT	ii
LIST OF FIGURES	vi
LIST OF TABLES	viii
ACKNOWLEDGEMENTS	ix
1 Introduction	1
1.1 Overview	1
1.2 XFELs	2
1.2.1 Microcrystals	3
1.2.2 TR-SFX and MISC	3
1.3 Microspectrophotometer	4
2 Software to Aid Experiments at XFEL	5
2.1 Software Solutions for the Synchronization of the MSP	5
2.1.1 Introduction	5
2.1.2 Performing Spectroscopic Experiments	8
2.1.3 Spectrometer Calibration	12
2.2 Hitfinder	13
2.2.1 Description	14
2.2.2 Determining Diffraction	16
2.2.3 Hitfinder Program	17
2.2.4 Hitfinder GUI	17
3 Experiments at XFEL	19
3.1 BlaC and MISC	19
3.1.1 Introduction	19

3.1.2 Methods	20
3.1.3 Results and Discussion	23
3.2 Phytochrome	27
3.2.1 Introduction	27
3.2.2 Methods	30
3.2.3 Results and Discussion	31
4 Conclusions and Outlook	35
5 References	37
Appendices	42
Appendix A: MAX-302 Xenon Light Source	42
Appendix B: Opolette Nanosecond Laser	46
Appendix C: Shutters	50
Appendix D: Fiber-Coupled LED	52
Appendix E: DG645 Digital Delay Generator	54
Appendix F: Andor SOLIS, Shamrock, and iStar	56
Appendix G: iStar Acquisition Types	62
Appendix H: Procedure for Taking Single Spectra	63
Appendix I: Laser Program Parameters	64
Appendix J: Hitfinder Code Listings	66

LIST OF FIGURES

Figure 2.1 Schmidt Lab Microspectrophotometer -----	6
Figure 2.2 Diffraction Patterns Analyzed by the Hitfinder Program -----	14
Figure 2.2 Hitfinder GUI -----	18
Figure 3.1 Nitrocefin and Ceftriaxone Chemical Structures -----	21
Figure 3.2 Powder Diffraction and Nitrocefin Tests on BlaC -----	23
Figure 3.3 BlaC Experiment Results -----	24
Figure 3.4 Biliverdin Chromophore -----	28
Figure 3.5 Fruiting Body Formation in <i>S. aurantiaca</i> -----	29
Figure 3.6 Reaction Initiation in SaBphP1-PCM-T289H Microcrystals -----	32
Figure 3.7 Laser Bleaching and Reaction Initiation Tests -----	33
Figure 3.8 Models of PHY Domain During Pr-Pfr Switch -----	34
Figure A.1 GOEGUI - Max-302 Control Utility -----	42
Figure B.1 OPOTEK Laser Control Software -----	48
Figure C.1 GOEGUI - ThorLabs Shutter Control Utility -----	50
Figure E.1 GOEGUI - DG645 Digital Delay Generator Control Utility -----	54
Figure F.1 Andor SOLIS - Shamrock Display Bar -----	56

Figure F.2 Andor SOLIS - Setup Acquisition	58
Figure J.1 MarCCD Image Class Constructor	66
Figure J.2 MarCCD Image Class Read Function	67
Figure J.3 MarCCD Image Class Average Function	67
Figure J.4 MarCCD Image Class Outlier Function	68
Figure J.5 Hitfinder Program Main Function Parallel Loop	69
Figure J.6 Hitfinder Program Spot Count Function	70

LIST OF TABLES

Table A.1 Max-302 Filters -----	45
Table C.1 ThorLabs Shutter Modes -----	51
Table D.1 LED Driver Modes -----	52
Table F.1 iStar Acquisition Modes -----	59
Table F.2 Setup Acquisition - Setup CCD Tab -----	60
Table F.3 Setup Acquisition - Setup Gater Tab -----	61
Table G.1 iStar Acquisition Types -----	62
Table H.1 Procedure for Taking Single Spectra -----	63
Table I.1 Laser Program Parameters -----	64
Table I.2 PYP Time Series Example Parameters -----	65

ACKNOWLEDGEMENTS

First, I would like to thank my advisor Professor Marius Schmidt for his support and guidance during my time in his lab. I have learned a lot in this time and I am grateful for the opportunity. I am also thankful for those that I have worked with in the Schmidt Lab over the past few years. Working with all of you has made the research fun despite being hard work. I wish good luck to all of you in the future.

To my committee members, Professor Peter Schwander and Professor Valerica Raicu, thank you for your input on this thesis. You have helped me finalize this work into a text worthy of presenting.

I also wish to thank the staff at the national laboratories that I have visited: APS, LCLS, and SACLA. My visits to these facilities were incredible opportunities and excellent experiences. It is thanks to your hard work that we could complete our research.

To everyone that I worked with as part of the BioXFEL STC, thank you for making me feel welcome in the community. I will remember the times that we were able to come together and share our experiences fondly. I wish you the best of luck on your own endeavors.

Lastly, I dedicate this work to my friends and family. Especially to my parents, Joe and Laurel Norwood, who have supported me from the beginning. Thank you for always believing in me. To my friends who are always by my side, thank you for pushing me to strive to be the best that I can be. I am who I am because of you all.

1 Introduction

1.1 Overview

Macromolecular X-ray Crystallography uses X-rays to determine the structure of proteins. While important, the structure of a protein is not enough to understand the protein's function. It is desirable to measure the structure of a protein during the time it is carrying out its task. This can be achieved by performing a time-resolved (TR) experiment where a reaction is started in crystals (see below) and the structures that evolve are determined by short X-ray pulses.

Prior to 2009, the brightest X-ray sources in the world were 3rd generation synchrotrons such as the Advanced Photon Source located at the Argonne National Laboratory located in Argonne, Illinois (Graber et al., 2011). These facilities are capable of measuring static and time-resolved protein crystal structures. Over the last few decades, experimental time resolution on the order of 100 picoseconds has been achieved at these synchrotrons (Cho et al., 2010; Schotte, 2003). Yet with a time resolution in the 100-picosecond regime, it was not possible to measure fundamental motions that happen on even faster time scale.

Starting a reaction in a time-resolved experiment can be difficult. Some proteins are sensitive to light and reactions are easier to initiate for example by a short optical laser pulse. Unfortunately, many interesting enzymatic reactions are not inherently light sensitive. They can be engineered to be light sensitive by using 'caged' substrates which are inactive until activated by a light pulse (Adams & Tsien, 1993; Ursby et al., 2002). However, the extra steps required by

this method take up time and often result in only a small amount of substrate being activated. These challenges prevented widespread application of this method.

With the advent of the world's first hard X-ray Free Electron Laser(XFEL) facilities within the last decade, the field of macromolecular X-ray crystallography has changed dramatically. Capable of femtosecond time resolution, XFEL experiments can measure faster processes than ever before. The nature of these experiments also allows for mixing substrate 'on-the-fly' just before exposure to the X-ray beam, which makes measuring enzymatic reactions much easier. The techniques developed for the XFEL have even been applied at synchrotrons in order to allow experiments at these more accessible facilities. The introduction of XFEL's has and continues to improve the field of macromolecular crystallography.

1.2 XFELs

The Linac Coherent Light Source (LCLS), located at the Stanford Linear Accelerator Center (SLAC) in Menlo Park, California is the first hard XFEL source in the world (Emma et al., 2010; W. E. White, Robert, & Dunne, 2015). The Spring-8 Angstrom Compact free electron LAser (SACLA), located at the Spring-8 Accelerator and Synchrotron Complex in Harima, Japan is the first XFEL to use superconducting technology to accelerate electrons (Kato et al., 2012; Pile, 2011). The European XFEL (EuXFEL) located outside Hamburg, Germany currently has the highest maximum energy and pulse rate of any XFEL (Cartlidge, 2016). In the coming years, even more facilities will open around the globe.

1.2.1 Microcrystals

The intensity of the XFEL is so great and can be focused to such a small spot that a single X-ray pulse would destroy the material in its path. This means that traditional crystallography methods are not employable when using an XFEL and new methods must be developed.

Despite the massive radiation damage to the crystal, the incredibly short pulses allow diffraction to occur before the crystal is damaged (Neutze, Wouts, van der Spoel, Weckert, & Hajdu, 2000). The high intensity of the XFEL also allows for the use of crystals much smaller than those traditionally used. These crystals are on the scale of micrometers (microcrystals) or even less. A complete dataset requires millions of diffraction images and therefore just as many crystals. Fortunately, microcrystals are often much easier to grow than macroscopically large crystals (Boutet et al., 2012).

1.2.2 TR-SFX and MISC

Time-Resolved Serial Femtosecond Crystallography (TR-SFX) (Pande et al., 2016; Tenboer et al., 2014) obtains diffraction images serially from a stream of microcrystals using the fs pulses of an XFEL after a reaction is initiated in these crystals. Because each image is obtained from a new crystal, TR-SFX is able to study irreversible processes in a way that traditional crystallography cannot. Mix-and-Inject Serial Crystallography (MISC) is a TR-SFX method which studies irreversible enzymatic reactions by mixing substrate with the stream of microcrystals (Kupitz et al., 2017). Special mixing-injectors designed to mix substrate and crystals are used to deliver crystals to the XFEL beam at a specific time after mixing occurs (Calvey, Katz, Schaffer, & Pollack, 2016). The use of microcrystals makes a MISC experiment feasible, since substrate will

diffuse into microcrystals more quickly and more completely than larger crystals (Schmidt, 2013). With diffusion times much faster than desired time delays, data collection can proceed efficiently with the potential of collecting an entire time series during run-time of the reaction with tens of time points.

1.3 Microspectrophotometer and Micro-Focus X-ray Source

The number of XFEL facilities in the world is quickly increasing, but operating an XFEL is expensive and access to them is highly competitive. It is especially important to perform pre-experiment characterizations before taking a sample to the XFEL. Running extensive tests beforehand removes as much uncertainty from the actual experiment as possible. The type of pre-experiment tests done depends on the nature of the experiment. In general, they should confirm important details before the actual beamtime. Preliminary tests for diffraction can be done with single crystal and powder pattern experiments. The Schmidt Lab performs these tests on a micro-focus X-ray source. Spectroscopic tests can isolate important time points, verify spectral change after specific stimuli, and reveal differences in behavior between solution and crystal. In the Schmidt Lab, time-resolved spectroscopic experiments in the ultra-violet and visible light range (TR-UV/VIS) are carried out on a MicroSpectroPhotometer (MSP) (Purwar, Tenboer, Tripathi, & Schmidt, 2013). There, a collection of software solutions is described, which I helped to design and develop, to run time-resolved experiments on this machine. An outline of the software as well as a description of operational procedure is provided here in chapter 2 and appendices A through I with the purpose of serving as a reference for future

generations of students and explaining the current features as a starting point for the development of new features.

2 Software to Aid Experiments at XFEL

2.1 Software Solutions for the Synchronization of the MSP

2.1.1 Introduction

Microspectrophotometer

The Schmidt lab has assembled a combination of various pieces of equipment which together function as a microspectrophotometer (MSP) (Purwar et al., 2013) which the lab uses to take time-resolved spectral measurements of proteins.

The MSP, pictured in Figure 2.1, takes spectra by means of pump-probe absorption spectroscopy. Opotek's Opolette 355 tunable laser is used as the pump, and Asahi Spectra's MAX-302 Continuous Wave Xenon light source is used as the probe. The spectra themselves are taken by Andor's Shamrock spectrometer and iStar camera. Thorlabs' Fiber-Coupled LED's are used as an additional wavelength-specific light exposure to reset protein conformation. Ocean Optics' HG-1 Calibration Source is used to calibrate the Andor spectrometer. Thorlabs' Shutter Controllers are used to block the laser and xenon light for both safety and timing. Stanford Research Systems' DG645 Digital Delay Generator ties each of the components together and regulates the timing of each to carry out time-resolved experiments. Optionally, Oxford Instruments' CryoJet can be used to regulate temperature of the sample. These machines will

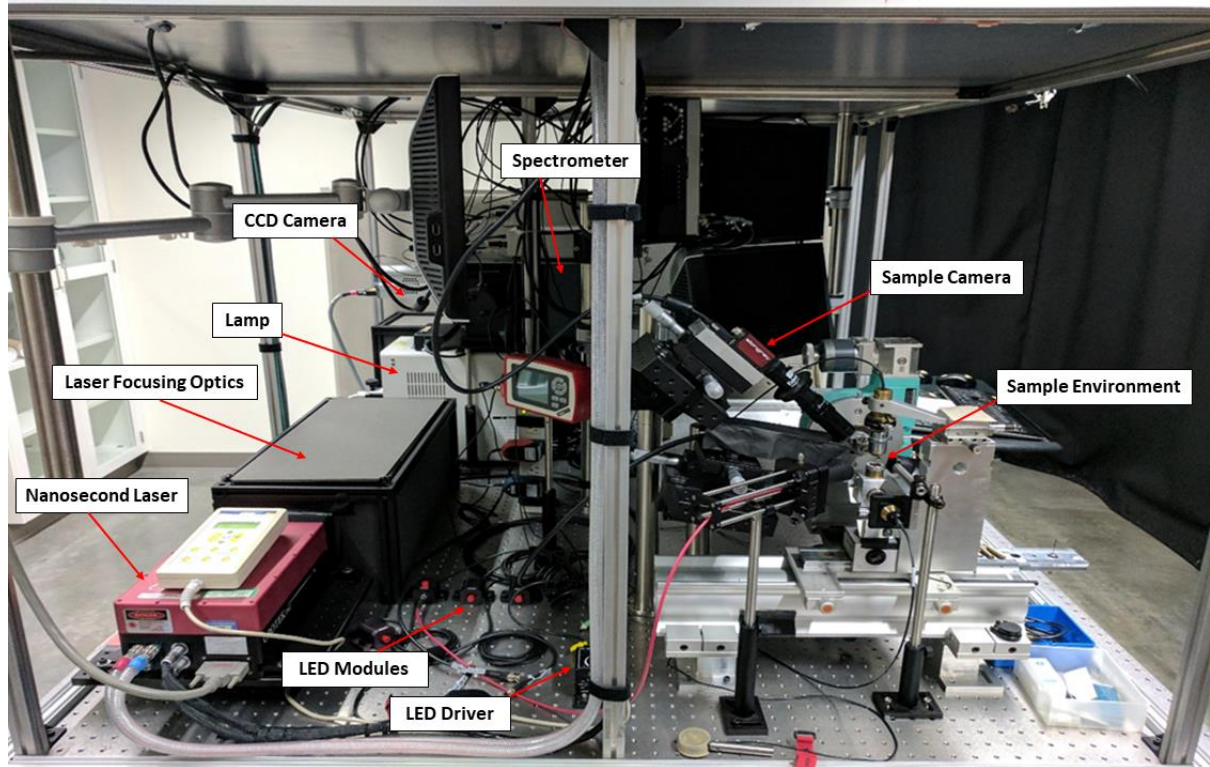


Figure 2.1 Schmidt Lab Microspectrophotometer. The MSP is located in the Kenwood Interdisciplinary Research Complex (KIRC) Room 4015.

work together to take spectra, but understanding how they function on their own is especially important as well.

The MSP is located on the right half of KIRC 4015 (upon entering the lab). As one of the components is a class 4 laser, which is capable of serious injury, the MSP is housed within a black-out curtain. When the laser is in use, this curtain should be closed and the 'Laser in Use' sign should be lit.

This chapter contains an overview of the knowledge pertinent to operating the MSP. A more detailed description of the machines and operational procedures are described in Appendices A-I. While they cover a good amount of information on the individual machines and their functions, it is not a suitable replacement for the knowledge gained from reading each

machine's individual manuals. Anyone operating these machines should read through each of those manuals first. Then, this chapter should be used to learn specific information gathered over time which may not be present in the official manuals.

GOEGUI, a Versatile Graphical User Interface for Operating the MSP

Most of the machines (where possible) have had software written to communicate with them through individual Graphical User Interfaces (GUIs). For the MSP, these GUIs were combined into one program, GOEGUI (GUI Of Everything GUI). GOEGUI was developed by myself and Jason Tenboer (UW-Milwaukee). GOEGUI can connect to the following machines: MAX-302 Xenon Light Source, Liquid Nitrogen CryoJet, DG645 Digital Delay Generator, Xenon and Laser Shutters, Shamrock Spectrometer, and iStar CCD camera. While GOEGUI can connect to the Shamrock and iStar, currently, it can only change the settings of these machines. GOEGUI cannot take spectra. For now, the program Andor SOLIS (available with the spectrometer) must be used to carry out experiments. The Opolette laser has its own control program that could not be assimilated into GOEGUI. It is not possible for a computer to communicate directly with the LEDs or the calibration source, nor is it necessary.

Operation Outline

The procedure for getting the MSP ready for a time-resolved experiment is as follows:

1. Turn on the Shamrock power unit.
2. Turn on the Max-302 Xenon Light Source using the switch on the back.
3. Turn on the Xenon and Laser Shutters by turning the power keys.
4. Turn on the DG645 Digital Delay Generator using the switch on the front.

5. Turn on the ICE450 by turning the power key
6. Turn on the Laser Electronics box using the switch on the front.
7. Open GOEGUI.
8. Connect to the Max-302 under the connections tab.
9. Turn on the Max-302 Lamp.
10. Open the OPOTEK laser software and start the flashlamp.
11. Open the Andor SOLIS program

Now the MSP is ready for alignments and for acquisition parameters to be set up in Andor SOLIS. Once the flashlamp warms up, the MSP will be ready to start a time-resolved experiment.

2.1.2 Performing Spectroscopic Experiments

Taking Single Spectra

A common type of spectroscopy experiment involves taking a spectrum which shows the absorbance of the sample. This experiment is not time-resolved.

To take a spectrum in Absorbance Units, the program also needs to collect Background and Reference data. Background data is taken without light falling onto the CCD to account for background noise. Reference data is taken with light through just the sample buffer to account for the absorbance of both the solution and the environment in which the sample is held. The Acquisition Types are further described in Appendix G (Tab. G.1). The general method for taking single spectra is described in Appendix H (Tab. H.1).

If the Acquisition Setup is changed before acquisition is fully completed, the signal window needs to be cleared and the experiment started from the beginning. The Background and Reference depend on these values as well and will not match the signal correctly otherwise.

When a Reference is taken, a warning will pop up saying that the settings have changed even when they haven't. Checking the box will keep the warning from popping up every time a Reference is taken. Every time the program is opened, the box will pop up when taking the first reference. It will have to be checked each time.

The shutter that blocks the xenon lamp light (xenon shutter) should not be left open for a long time while the sample is being aligned. For the most part, the xenon lamp light that probes the sample shouldn't affect the sample too much, but long exposure to the light could damage the sample. To be on the safe side, the shutter should be opened immediately before taking the signal, and closed immediately afterward.

Taking Time-Resolved Spectra

The other common type of spectroscopy experiment done with the MSP is a time-resolved experiment. The laser is used to initiate a reaction in the sample and spectra are taken at a certain time after the laser hits. A program written in the Andor Basic Language for use in SOLIS is used to run the experiment.

There are a few different versions of the Laser Program. Currently, the one to use is called Current_Andor_Program. There are versions for different proteins with certain

parameters saved. To create a new setup, a copy of Current_Andor_Program_Template can be made with changes to the parameters as needed.

The user should read through the Current_Andor_Program and try to understand how it works. Essentially, the program runs the same method as described above for single spectra, except the program is capable of taking many spectra for an entire time series. Additionally, the program connects to the DG645 delay generator to regulate the timings of the laser and iStar camera.

Before, using the program required changing many variables which were spread throughout the code. I rewrote the program so that the variables that may need to be changed are all located at the beginning. The rest of the functions should only be altered in order to write a new type of experimental setup or change the current one.

The parameters which are defined at the start of the program may need to be changed regularly, depending on the experiment. These parameters are described in Appendix I (Tab. I.1). It is likely that they will not need to be changed at all, unless a new kind of experiment is being created. If the COM port numbers change for the shutters and DDG, the COM port number variables will have to be set to the new values.

When the program runs, it will first prompt for a directory. This is a subfolder of the Main data folder that is specified with RootPath\$. Then, it will prompt for a filename. This will be the root filename of each image taken in the series. With these two values entered, some of the data from the program will be printed in the output window. This is the time to check these

values to make sure they are entered correctly. The program offers a chance to quit if some parameters need to be changed, or to continue if everything is correctly set.

Now the program will make COM port connections, and set the DDG, iStar, and Shamrock according to the values given in the program. When the connections have been made, the program will pause request that the dilution buffer be positioned in order to take the background and reference spectra. After the background and reference spectra are taken, the program will pause again to request the sample now be positioned at the intersection of the Xenon light source and the laser.

A 'dark before' spectrum is a regular spectrum taken without laser exposure/excitation. It is used to compare the change in absorbance due to the laser exposure by comparing with the signal spectra. A 'dark after' spectrum is a regular spectrum taken after all laser exposures. It is used to determine if laser exposure has prevented the sample from returning to its original state after laser exposure (referred to as bleaching). Signal spectra are taken just after each laser flash to measure the absorbance caused by laser exposure.

Before each spectrum is taken, the program will pause to recommend that the sample be manually exposed to light from an LED. This will allow the sample to be exposed as long as is necessary, but it has to be turned on and off by hand. If the sample does not need to be exposed to LED, this step can be skipped.

The laser should be switched on at some point before the program declares that it will be taking the signal spectra. It can be activated just after the Dark Before spectrum is taken or at the beginning of the experiment. Since the laser will be set to external mode, the laser will

only send pulses when the DDG instructs it to, and the laser shutter will only open when taking the signal spectra. Still, at this point, safety goggles should be worn when beginning the experiment and the safety curtains should be closed.

Once the Dark After spectrum has been taken, the program has finished and all images should be saved. The laser can be turned off at this point. It should be confirmed that the shutters have closed correctly before removing goggles or opening the curtain.

2.1.3 Spectrometer Calibration

The basic function of the spectrometer is to measure counts, that is, the number of photons which fall on each pixel of the iStar camera's Charge Coupled Device (CCD). To measure Absorbance Units by wavelength, the spectrometer must be calibrated by entering which pixels should correspond to which wavelengths. To do this, the Ocean Optics Mercury Argon Calibration Light Source is used. The spectra produced by Mercury-Argon lamp light has strong peaks at certain known wavelengths. By projecting the light on to the iStar camera, using the spectrometer, SOLIS can be used to pick a pixel number where a peak occurs and specify the wavelength it should be for a number of peaks. This allows the program to create a calibration file and show the spectra in terms of wavelengths instead of camera pixels. Specific instructions on using the program to calibrate the spectrometer can be found in the Calibration section in the Andor User Manual.

In order to take an image of the Calibration Light Source's light, the fiber carrying the Xenon lamp's light must be removed from the F/# matcher's mirror tube (the black cylinder extending from the Shamrock which contains lenses or mirrors to focus light from the fiber on

the CCD chip) and replaced with the fiber from the Calibration Light Source. When calibration is finished, the xenon fiber light must be repositioned. Whenever a new fiber is placed, it's emerging light must be focused. Focusing the fiber light mainly comes down to tightening the fiber in the holder at the right height such that the mirrors in the F/# matcher align the light on the CCD with the greatest intensity. This is done by setting the Acquisition Mode to Real Time, Readout Frame as Image, and Readout Time Per Pixel to 1. Upon pressing Take Signal, a real-time image of the light falling on the CCD is displayed. To focus the light, the height of the fiber in the fiber holder needs to be adjusted until it is at its brightest, then locked in place with the set screw.

Depending on the type of fiber connector, the fiber may be one large circular spot, or a line of smaller circular spots. If it is the latter, the fiber can be rotated as well so that the spots are aligned vertically on the CCD. The light should also be at the center of the CCD. To align the position of the light the F/# matchers will have to be re-aligned as well. To do so, follow the instructions in the Technical Packet: [F/# Matchers for the Shamrock SR303i, SR500i and SR750](#) (the Schmidt Lab has the SR303i).

2.2 Hitfinder

Serial crystallographic experiments expose a stream of small crystals to X-ray pulses. The tiny crystals arrive in a random sequence, so that not every X-ray pulse hits a crystal. Even with pulse repetition rates of 120 Hz, the beam is only able to probe a tiny fraction of the jet volume. Nevertheless, a large number of jet volumes are exposed to the beam. The image collected on a X-ray sensitive, pixelated area detector is then called a diffraction pattern. Many images

contain Bragg reflections when a crystal is hit (Fig. 2.2a). Others contain only scattering from the jet (blank images, Fig. 2.2b) without Bragg reflections when the spaces between crystals are exposed. The percentage of images containing Bragg spots versus the total number of images collected (hit rate) is often on the lower side, usually smaller than 10%. Blank images therefore constitute the majority of collected images in a serial experiment, which must be separated from the hits by a hitfinder. Since hitfinders were developed mainly for XFEL diffraction patterns, we found it necessary to develop a hitfinder for processing serial Laue data collected at a synchrotron.

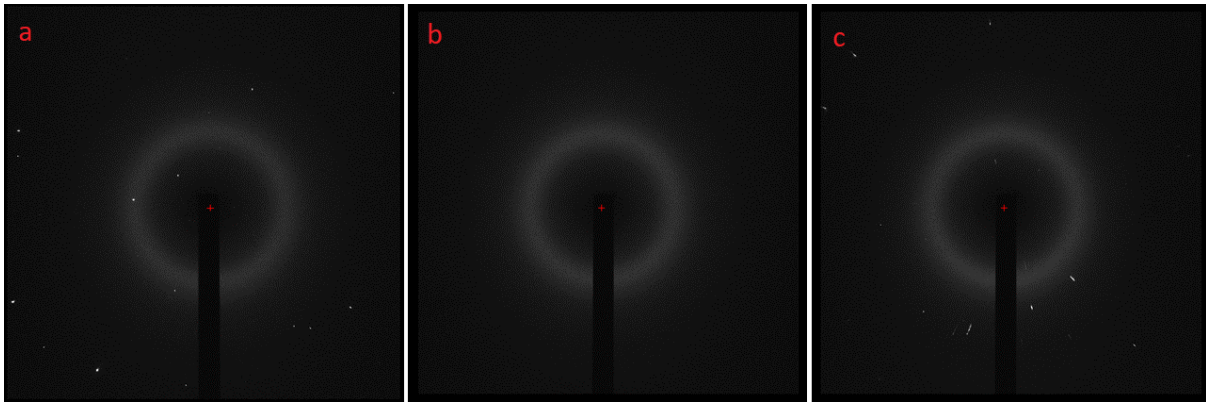


Figure 2.2 Diffraction Patterns Analyzed by the Hitfinder Program. (a) An image which contains Bragg diffraction spots. (b) A blank image which contains no Bragg Spots. (c) An image which contains Bragg diffraction, but the spots are streaky.

2.2.1 Description

The hitfinder program is a console program written in C++ and developed by myself. The program was designed to read diffraction pattern images taken with a MarCCD detector, read them into memory, and determine whether diffraction was present. In order to simplify reading in the data for each image, the MarCCD Image Class was written. The Image Class defines the rules for creating an object which holds a diffraction pattern's data in the program. A MarCCD diffraction pattern is a picture in binary format which is composed of two sections. The first

section is a header which contains information about the image such as pixel height, pixel width, and detector distance. The second section contains the data for the image itself encoded as unsigned 16 bit integers which represent the intensities measured by the detector CCD pixels. The Image Class saves the useful header values and a two-dimensional array of the image data as object fields. Each diffraction pattern which is read in as an Image Object has its own record of these variables stored.

Diffraction patterns do not just record either intensity in diffraction spots or no intensity at all. There is always some background intensity present. Usually diffraction spots contain pixel intensities which are much higher than the background, but sometimes weaker spots will have an intensity only just slightly above the background. Showing that these spots constitute diffraction as well proves more challenging. The goal was to find a quick way to identify if a pixel intensity is above the background. The method that I chose came from simple statistics involving outlier values (Tukey, 1977). By calculating the Interquartile Range (IQR) of the set of pixel intensities, the upper boundary between appropriate values and outliers can be determined. Assuming the background approximates a normally distributed data set, pixels which correspond to diffraction spots will be outliers.

Once it has been determined that outlier intensities representing potential Bragg reflections are present in the image, it is also necessary to ensure that the pixels are arranged together as spots. This is done by scanning the image and checking that the pixels around any outlier pixels are also outlier pixels. Currently, a spot size is given by the user which corresponds to the number of outlier pixels which must be arranged in a square to be considered a spot.

This method over-counts spots since a number of these squares can be found in a spot if the

given spot size is small enough. A more accurate peak-finder could be written using a more intensive algorithm to determine the actual size of each spot encountered in the image. However, the additional steps compromise the speed of the hitfinder. Since blank images (those without reflections) will not contain spots to over-count, over-counting should have no effects on removing the blank images.

2.2.2 Determining Diffraction

Since the atomic form factor declines with the scattering angle, the background due to unspecific scattering is very low at the edges of the images. Due to the sheer number of low intensity pixels, the average remains rather low regardless of whether diffraction spots are present. Since these pixels represent lower intensity than the rest of the background, they surely don't represent diffraction spots. Therefore, in calculating the upper outlier range, it is safe to consider only pixels which are greater than the average without any loss of generality.

The IQR is the difference between the first and third quartiles, which are the medians of the upper and lower halves of the set. After removing the values below the average, the remaining number will be different for any given image and so the method for calculating the quartiles must take this into account. With the IQR known, an outlier is a number which is greater than the third quartile plus three times the IQR. This factor of three is arbitrary, but generally accepted. It would be possible to change it as another hit-finding parameter if so desired.

2.2.3 Hitfinder Program

The hitfinder program quickly determines the hit status of many images by reading them in parallel. The parallel threads are managed using the OpenMP (OMP) Library (Chapman & Massaioli, 2005). Once the arguments and other important variables are set, the desired number of threads are opened and a parallel loop is started which each thread runs at the same time (Appendix J Fig. J5). The different jobs that the threads do is determined by their thread id. The master thread (thread id 0) has the job of reading images into memory using the MarCCD Image Class and placing them into the images array to be accessed by the other threads (worker threads). Once the array is full, the master thread waits for confirmation from the worker threads that an image has been processed and can be replaced by a new image in the array.

The worker threads access the element of the images array which matches its thread id. Each worker thread then calculates the image's average, outlier value, and spot count (Appendix J Fig. J6). If the spot count is greater than the given threshold, it is added to the list of images which are considered hits (hit list). A status report is sent to the standard output stream for monitoring progress while the program is running. The value in the done array which corresponds to the thread id is changed, signaling to the master thread that the worker thread is ready for a new image.

2.2.4 Hitfinder GUI

The hitfinder GUI (Fig. 2.3) was written in Python. The first tab (Fig. 2.3a) allows users to input hit-finding parameters more easily than as command line arguments. The GUI calls the

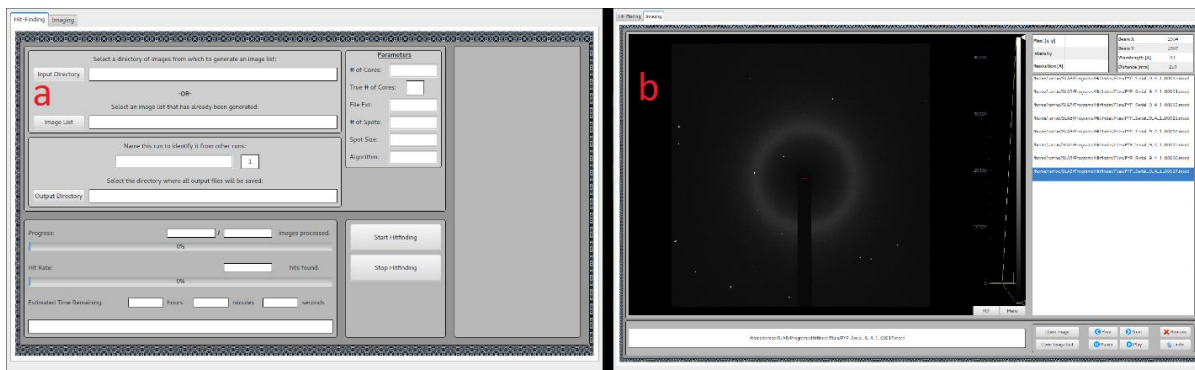


Figure 2.3 Hitfinder GUI. (a) The hit-finding tab contains forms to assist the user in setting up a hit-finding run. (b) The imaging tab contains an image viewer designed to easily view images from the lists derived from hit-finding runs.

hitfinder program with the desired parameters as arguments and uses the information from the standard output stream to update the status bars in the GUI.

The second tab (Fig. 2.3b) provides a module for displaying an image of the binary diffraction patterns. Images can be viewed separately or as part of a list, namely the hit lists produced by the hitfinder program. If desired, an image can be removed from the list. This would be done if an image contains diffraction but is of bad quality (Fig. 2.3c). A repeating pattern of hit-finding, removing images by inspection, and hit-finding again with stricter parameters can reduce a large set of images down to one which contains only images with diffraction.

3 Experiments at XFEL

3.1 BlaC and MISC

3.1.1 Introduction

Our team travelled to the XFEL located at the LCLS in Menlo Park, CA on December 8, 2015 and September 9, 2016 to perform 2 experiments on BlaC. My role in these experiments was to assist in data processing and sample loading. Results from the XFEL experiments are listed, however very shortly below, since I have been involved only marginally in the interpretation of the crystallographic data.

BlaC is a β -lactamase enzyme which is synthesized by the Tuberculosis (TB) causing bacteria *Mycobacterium tuberculosis* (MTb) (Voladri et al., 1998; Wang, Cassidy, & Sacchettini, 2006). BlaC confers to TB resistance against β -lactams, an important family of antibiotics so named for the β -lactam ring they each exhibit. Mtb BlaC catalyzes the opening of the β -lactam ring by means of a nucleophilic attack by an active site serine residue, resulting in an acyl-enzyme intermediate (Boyd, Herron, Lunn, & Spitzer, 1980; Dub  e et al., 2012). The inactive open-ring product is then generated from the intermediate by hydrolysis of the ester bond (Jeon et al., 2015; Tremblay, Fan, & Blanchard, 2010). Previous studies have classified Mtb BlaC as an extended spectrum β -lactamase (ESBL) which is capable of hydrolyzing all classes of β -lactams (Babic, Hujer, & Bonomo, 2006; Hugonnet & Blanchard, 2007).

Due to the presence of Mtb BlaC, β -lactam antibiotics have not been systematically used as a treatment for TB (Tremblay et al., 2010). A different class of strong antimycobacterial

antibiotics was developed, but certain strains of TB have since become extensively drug resistant (XDR-TB) (Hugonnet, Tremblay, Boshoff, Barry, & Blanchard, 2009; Tremblay et al., 2010). With these new resistances, TB remains a formidable infectious disease with 6.1 million new cases reported in 2015 (WHO, 2016). These bacteria often utilize multiple kinds of β -lactamases to gain a broad-range resistance similar to that conferred by Mtb BlaC (Bush & Fisher, 2011). A detailed and time-resolved observation of how Mtb BlaC hydrolyzes the β -lactam ring could lead to new methods of treating both TB and other β -lactam resistant bacterial infections.

3.1.2 Methods

It is impossible to tell how well a crystal will diffract based only on how it looks. Therefore, diffraction should be confirmed before an experiment. With single crystals, this is easy to do using either a home source or a synchrotron. It would be difficult, however, to test the diffraction of a single micron-sized crystal. It is possible to test the diffraction of microcrystals using a technique which is similar to X-ray powder diffraction (XRD). In XRD, a large number of crystals are crushed into a fine powder which is then subjected to X-rays. The resulting diffraction pattern forms rings from which structural information about the crystal can be deduced (Bish & Post, 1989). In a microcrystal powder pattern, the random orientation of each crystal in a slurry of microcrystals causes diffraction rings to form in the same way. Structural information, or even just the presence of diffraction can be obtained from these powder patterns.

It was also desired to confirm the diffusion time of substrate into the microcrystals. Due to the way that proteins must arrange themselves to form crystals, it is likely that diffusion pathways and therefore diffusion times in crystal and solution will differ. Nitrocefirin, a cephalosporin-like substrate with a β -lactam ring, is susceptible to attack by β -lactamase enzymes (Fig. 3.1a). The presence of β -lactamase enzymes can be detected by a color change from yellow to red following the hydrolysis of the ring. (Chantemesse et al., 2017; Chow, Xu, & Blanchard, 2013) In order to measure diffusion time, the Schmidt Lab MSP was used to watch the spectral change of the nitrocefirin as it changed colors.

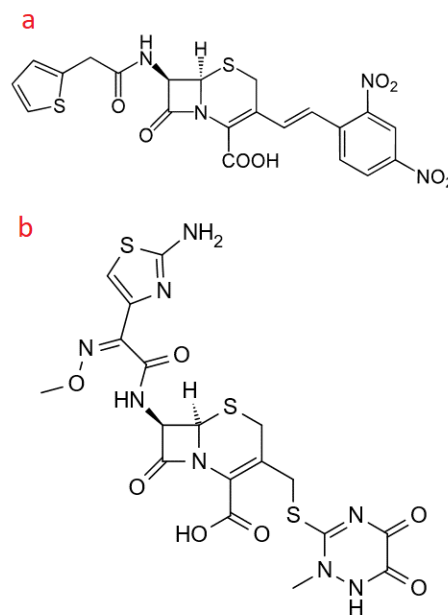


Figure 3.1 Nitrocefirin and Ceftriaxone Chemical Structures. (a) Structure of Nitrocefirin, a cephalosporin-like substrate which contains a β -lactam ring. Wikimedia Commons / Public Domain. (b) Structure of Ceftriaxone, a third-generation cephalosporin antibiotic. Wikimedia Commons / Public Domain.

Our team carried out two MISC experiments with BlaC at the Coherent X-ray Imaging (CXI) (Liang et al., 2015) instrument at the LCLS. The first provided proof of concept for the MISC method employed at an XFEL. The second showed that the MISC method is able to obtain structures of enzymatic reactions in process. These experiments used the third-generation cephalosporin antibiotic ceftriaxone (CEF, Fig. 3.1b) as the substrate for its longer turnover rate ($r=1.22s$).

In the first experiment, crystals were produced by Free Interface Diffusion (FID) using 50 μ l of 120-150 mg/mL protein and 500 μ l of 2.4 M ammonium phosphate (PH 4.1) as precipitant. Crystals began to form over the course of 20 hours, but after 30 hours had grown to over 20 μ m

in length. Using 100 μm glass beads and a vortex mixer, the crystals were crushed resulting in crystals approximately 3-10 μm in length. Mixing of the microcrystals and the antibiotic substrate (200 mmol/L) occurred in a simple T-Junction connector, suggested by Mark Holl (Arizona State University). The mixed sample were delivered to the XFEL beam by a Gas Dynamic Virtual Nozzle (GDVN). The setup of the nozzle and delivery line resulted in the mixed sample arriving at the beam 2 seconds after mixing began. Estimates of the diffusion time of CEF into the crystals were calculated to be less than 15ms, which is negligible in comparison. Two room temperature structures were measured for comparison, one with and one without mixing.

The second experiment used two different kinds of microcrystals, shards and needles, so named for their shapes. The shards were produced by Chris Kupitz (UW-Milwaukee) and Jose Olmos (Rice University) using phosphate as precipitant. The shards were developed from the same crystallization as in the first experiment. The needles were produced by Jose Martin-Garcia (Arizona State University) using PEG 1000 as precipitant. The sample and substrate (CEF, 200 mmol/L) were mixed and delivered by an injector (Calvey et al., 2016) which was designed to use different nozzles to change the amount of time between mixing and reaching the XFEL beam. With this setup, we were able to collect structures at 30ms, 100ms, 500ms, and 2s after mixing for each type of crystal.

Collected diffraction patterns were first analyzed by the program Cheetah (Barty et al., 2014) to find the ones that contain Bragg reflections. The CrystFEL (T. A. White et al., 2016) suite was then used to index and integrate those patterns. Data was merged to yield full reflection intensities. Programs from the CCP4 (Winn et al., 2011) suite were used to process

the data further. Structures were solved by molecular replacement by Suraj Pandey (UW-Milwaukee). The structures were determined to be tetrameric in the shards and monomeric in the needles (see results further below, chapter 3.1.3).

3.1.3 Results and Discussion

The powder patterns did not show definite diffraction, but some rings appeared to be faintly visible. An averaging program (developed by myself) was used to accumulate the images in an attempt to make the rings darker. Ultimately, these accumulations showed only weak diffraction (Fig. 3.2a). Diffraction of similar BlaC microcrystals was confirmed by J. Olmos and the Rice University team with a similar approach. Since the microcrystals are so small,

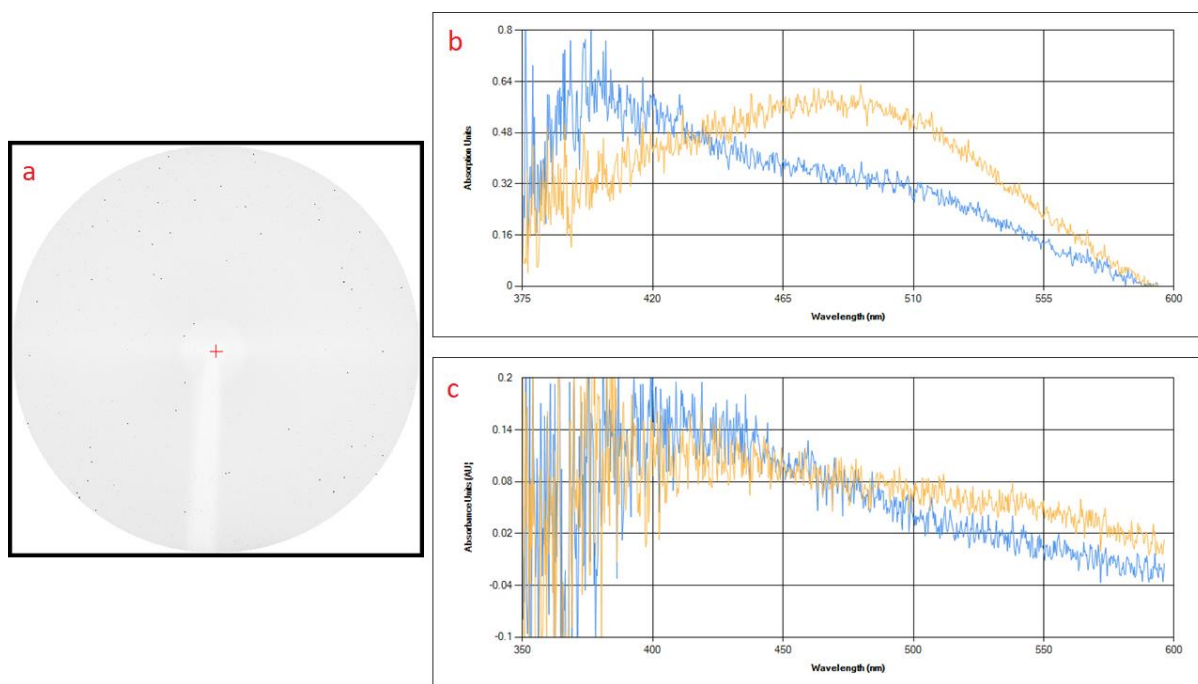


Figure 3.2 Powder Diffraction and Nitrocefin Tests on BlaC. (a) Accumulated BlaC Microcrystal Powder Pattern. The image is the result of adding up the intensity of many powder diffraction patterns from BlaC microcrystals taken with the Schmidt Lab micro-focus X-ray source. No discernable rings are present on this powder pattern. The beam center is marked in red. (b) Spectra of Nitrocefin Test on BlaC in Solution. A drop of nitrocefin was added to a drop of BlaC in solution. The blue line represents the absorbance of BlaC in solution without nitrocefin. The gold line is obtained 20 seconds after nitrocefin is added to the drop. A clear shift in the absorbance peak after 20 seconds is visible. (c) Spectra of Nitrocefin Test on BlaC microcrystals. A drop of nitrocefin was added to a slurry of microcrystals and placed between two slides. The blue line represents the absorbance of the BlaC crystals without nitrocefin. The gold line is obtained 10 minutes after the nitrocefin is added. A very slight change is visible after 10 minutes.

amplification of diffraction by the crystal lattice is diminished and thus more incident intensity is required to achieve detectable diffraction. It is possible that because the X-ray source at the Schmidt Lab was acquired in 2008, it no longer has the intensity to diffract from these small crystals.

The Schmidt Lab MSP (Chapter 2) was designed for light-initiated reactions and isn't particularly suited for studying time-resolved enzymatic reactions. The tests had to be performed by manually mixing a compound which reacts with BlaC and changes color. This compound, nitrocefin, was mixed into a drop of the sample in the sample stage area

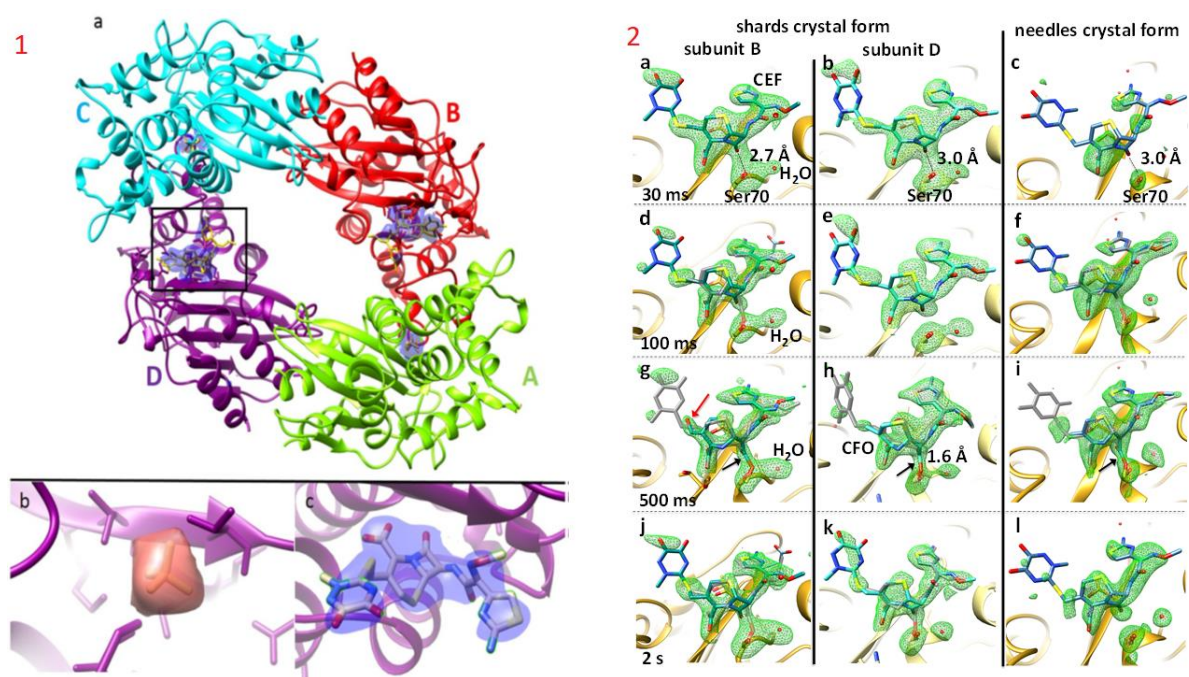


Figure 3.3 BlaC Experiment Results. (1) Electron Density in the Binding Pockets of BlaC. (a) Refined model of the full tetramer after mixing. Mixed Electron Density in the binding pockets is shown in blue. The box denotes the close-up of the binding pocket in subunit D shown in the rest of the figure. (b) Unmixed electron density of subunit D corresponding to bound phosphate is shown in red. (c) Mixed electron density of subunit D corresponding to ceftriaxone shown in blue with ceftriaxone model included. This figure is adapted from a figure in (Kuptitz et al., 2017) published in *Structural Dynamics* (2) Ceftriaxone Electron Density in BlaC Binding Pockets for different crystal forms and time delays. (a, b, c) Presence of electron density corresponding to the Enzyme-Substrate Complex in each crystal form at 30ms. (d, e, f) Electron density corresponding to intact ceftriaxone species is the majority at 100ms. (g, h, i) Electron density corresponding to opened-ring species of ceftriaxone is the majority at 500ms. (j, k) At 2s, a mix of intact and opened-ring species are observed in subunits B and D of the shards. (l) At 2s, electron density only indicates presence of intact ceftriaxone in the needles. This figure is adapted from a figure in (Olmos, Pandey, Martin-Garcia, et al. 2017) available on BioRxiv.

immediately before data collection. Future experiments of this type would benefit from a mixing/jetting component added to the sample stage area. As a comparison, tests were first done on BlaC in solution which changed color very quickly. A complete shift in the absorption peak occurs in under 20 seconds (Fig. 3.2b). Tests on the microcrystals show a change on longer time scales (> 10 min, Fig. 3.2c). The crystals are so thin that the optical path length through the crystals is small (~5 μm). To obtain significant signal, sufficient product must first accumulate. Monitoring the color change in the microcrystals by eye for much longer time periods revealed a faint color change. During the XFEL experiment, the CEF was at a much higher concentration than it was possible to concentrate the nitrocefin due to limited solubility. If the nitrocefin could be more concentrated, the concentration in the crystals would also be much higher and the product could actually be detected much faster by our MSP.

The reaction after mixing was analyzed by comparing mixed and apo structures (Fig. 3.3.1a). No substrate is present in subunits A or C, only a phosphate molecule is found (Fig. 3.3.1b). The packing of the crystals and the locations of their crystal contacts apparently prevent access to these binding pockets in a way that does not occur in solution. Electron Density (ED) is present in subunits B and D (Fig. 3.3.1c). This presence of ED shows that substrate can access the binding pocket and that binding occurred there. Since the 2 second time point is around twice that of the turnover time measured for ceftriaxone, one or two cleavings have already taken place. The ED collected at the 2 second time point likely shows a steady state composed of many intermediate states.

We sought to answer the questions about how crystal packing impacts the substrate's access to the binding pockets as well as the enzyme's ability to catalyze the substrate. To

achieve this, two different crystallizations of BlaC were used. The shards contain a tetramer in the asymmetric unit while the needles contain a monomer. The structure in each crystal type was measured at four different time points throughout the reaction and compared to the apo structure. There are both similarities and differences in the structures from the two different crystal forms.

In both types, binding of the substrate has already occurred before 30ms (Fig. 3.3.2a, b, c). At 100ms, around 30% of the CEF molecules have had their β -lactam ring hydrolyzed but most are still intact (Fig. 3.3.2d, e, f). At 500ms, around 70% of the molecules now have an open ring (Fig. 3.3.2g, h, i). At 2s, a steady state has been reached in the shards, just as in the first experiment (Fig. 3.3.2j, k, l).

Subunits A and C of the shards do not contain substrate, as in the first experiment. Measurements of the needles and subunit D of the shards are similar except that the needles have a lower occupation of substrate. This is likely due to the difference in enzyme concentration between the two crystal types. Since the CEF concentration outside of the crystals is the same in both cases, different enzyme concentrations result in different final CEF to enzyme ratios.

In the first experiment, the presence of electron density that corresponds to ceftriaxone in the binding pocket of the mixed sample indicates that room temperature MISC experiments on enzymes are possible. In the second experiment, structures from many time points show the reaction in process and confirms the steady state measured in the first experiment. These

results further demonstrate the ability of MISC experiments to measure enzymatically catalyzed reactions on the order of milliseconds.

3.2 Phytochrome

3.2.1 Introduction

Our team travelled to the XFEL located at SACLA in Japan on December 9, 2016 in order to perform an experiment on a phytochrome. My role in this experiment was assisting in data processing. As with the BlaC, I have been mainly concerned with collecting spectra, and was only slightly involved in the interpretation of the X-ray data. A brief outline of the experiment follows.

Phytochromes are a family of environmental light sensing proteins that control light-dependent responses in plants, fungi, and bacteria. Phytochromes regulate many developmental processes in plants such as seed germination, stem extension, and flowering (Bae & Choi, 2008; Hughes, 2013). In cyanobacteria, they can control the amount of chlorophylls that are synthesized depending on the wavelength of the environment's light (Gan et al., 2014). The presence of light-sensing phytochromes in photosynthetic organisms is expected, but less understood is how phytochromes function in non-photosynthetic bacteria in which they've also been found. These non-photosynthetic organisms can use phytochromes for many functions from light-dependent spatial positioning to controlling carotenoid expression as a way to change optical density and protect against light damage (Auldrige & Forest, 2011).

In general, phytochromes contain a c-terminal output domain (usually a histidine-kinase) and an n-terminal photosensory core. The photosensory core has a modular domain architecture which is composed of PAS (PER, ARNT, SIM), GAF (cGMP phosphodiesterase, adenylate cyclase, FhIA), and PHY (specific to the phytochrome) domains (Auldrige & Forest, 2011).

Phytochromes employ a linear tetrapyrrole (or bilin) as

their chromophore. The bilin is represented as phytochromobilin in plants (Lagarias & Rapoport, 1980), phycocyanobilin in cyanobacteria (Hughes et al., 1997), or biliverdin (BV) in bacteria (Bhoo, Davis, Walker, Karniol, & Vierstra, 2001; Tasler, Moises, & Frankenberg-Dinkel, 2005). The chromophore is covalently bound via thioether linkage to a conserved cysteine residue in either the PAS (bacteria) or GAF (cyanobacteria and plants) domain (Edlund et al., 2016). After light is detected by the chromophore, a series of structural changes switches the protein between a red light absorbing state (Pr) and a far-red light absorbing state (Pfr). These changes are triggered by a Z-to-E isomerization about the C15=C16 double bond of the chromophore (Fig. 3.4), structural changes of the chromophore binding pocket, and a refolding of the PHY domain sensory tongue. In some way, these changes then lead to the activation of the output domain, though the exact process is not yet fully understood (Burgie et al., 2014; Edlund et al., 2016).

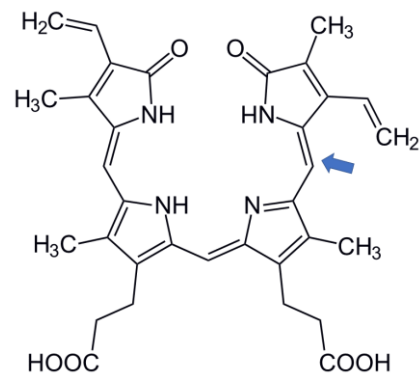


Figure 3.4 Biliverdin Chromophore. *SaBphP1-PCM-T289H* contains a biliverdin (BV) chromophore. The double bond about which the Z to E isomerization takes place is marked with an arrow. Wikimedia Commons / Public Domain.

Two bacteriophytochromes (BphPs) are found in the Myxobacteria *Stigmatella aurantiaca*, denoted SaBphP1 and SaBphP2. Our team carried out experiments on SaBphP1.

Myxobacteria experience a stage in their life cycle where they produce multicellular fruiting bodies (Fig. 3.5). In the non-photosynthetic *S. aurantiaca*, this process is stimulated by light and is dependent on wavelength. Due to the difference in fruiting body growth in red and far-red light, it is likely that these bacteriophytochromes are involved in this process.

SaBphP1 differs from classical BphPs in that it contains a threonine(Thr-289) instead of a conserved histidine(His) at position 289 in the GAF domain. In classical BphPs, the conserved His is important as it binds to ring D of the chromophore and stabilizes the Pr state. In order to understand the effect of this unusual replacement of an important conserved His, a mutant variant of SaBphP1 with the thr-289 replaced with His (T289H) so that it resembled a classical BphP was used. Additionally, the SaBphP1 chromophore binding domain (CBD, containing only the PAS and GAF domains) and the entire photosensory core module (PCM) were crystallized as separate versions of SaBphP1. To refer to the mutant type with the full photosensory core module, the name SaBphP1-PCM-T289H will be used.

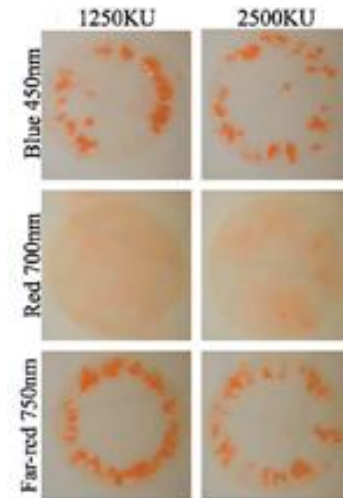


Figure 3.5 Fruiting Body Formation in *S. aurantiaca*. Comparison of fruiting body formation in blue (450 nm), red (700 nm), and far-red (750 nm) light. This figure is from an experiment performed in the Stojokovic Lab.

Crystal structures at synchrotrons are collected at cryogenic temperatures to protect against radiation damage. In an XFEL experiment, diffraction occurs before radiation destroys the crystals even at room temperature. This allows the dynamics of the enzymatic reaction to be measured in a biologically relevant state. I assisted in the XFEL experiment to collect a room temperature structure of SaBphP1-PCM-T289H mainly by processing data.

3.2.2 Methods

Switching between the Pr and Pfr states is associated with configurational changes of the central BV chromophore. This change, and in addition conformational and H-bond changes directly affect the absorption spectra. By measuring the absorption spectra before and after a light stimulus, a change in the absorption peaks can confirm that these conformational changes have taken place. In SaBphP1-PCM-T289H there are three absorption peaks, one main peak at 706 nm with two 'shoulder peaks' on either side (Fig 3.7b) The expected spectral change from Pr to Pfr is for the left two peaks to reduce in absorption while the right-most peak increases (Fig. 3.7b). The Schmidt Lab MSP (Chapter 2) was used to initiate the Pr-Pfr switch and measure the spectral changes with the goal of confirming light activation in the crystals which would be used at the beamline. SaBphP1-PCM-T289H both in solution and as microcrystals were tested to see if they reacted differently. Activation tests (Fig. 3.6) were done to see if light initiation occurred and bleaching tests (Fig. 3.7a) were done to see how much energy could be delivered to the sample before damage occurred.

Various SaBphP1 constructs of both CBD and PCM were cloned, overexpressed, and purified by the Stojkovic group at North Eastern Illinois University. Microcrystals of the SaBphP1-PCM-T289H were prepared in the Schmidt Lab by mixing 20 mg/mL protein in equal parts with a 0.1M MES (pH 6.2), 8-5% PEG 20,000 (w/v), 5.2% Acetonitrile (v/v) precipitant. The mixture stirred overnight and was left to rest for several days to let the crystals mature.

Room temperature X-ray data of SaBphP1 PCM T289H microcrystals were collected at beamline BL3 at SACLA. The crystals were concentrated to around 10^{11} crystals/mL and folded

into nuclear grade grease at a 1:10 (v/v %) ratio. The microcrystal-grease mixture was transferred into a reservoir up to 400 μl at a time and extruded into air through a 75 μm diameter nozzle at a flow rate of around 5 $\mu\text{l}/\text{min}$. This extruded stream was then exposed to intense X-ray pulses of under 10 fs with a repetition rate of 30 Hz.

Diffraction patterns were collected on an 8-module CCD detector (Kameshima et al., 2014) The patterns were analyzed with a user friendly data processing pipeline (Nakane et al., 2016) which accomplished hit-finding with Cheetah (Barty et al., 2014) and indexing and Monte Carlo integration by CrystFEL (T. A. White et al., 2016). The hit rate was about 15% and the indexing rate was about 53% yielding 36539 successfully indexed patterns. From these, partial intensities were extracted and merged into full reflection intensities. The full intensities were converted into structure factor amplitudes by means of software based on the CCP4 program suite (Winn et al., 2011). Structures were solved by molecular replacement by Suraj Pandey (UW-Milwaukee).

3.2.3 Results and Discussion

No spectral change was seen in the microcrystals from a single 660nm laser pulse (Fig. 3.6a). To test if a longer time was required to acclimate to the Pfr state, a 660nm LED was also used to initiate the reaction. With the LED, a slight spectral change was observed, but only in the left peaks. The right-most peak, which does see an increase when measured on a conventional spectrometer (Fig. 3.7b), shows no change when measured on the MSP (Fig. 3.6b).

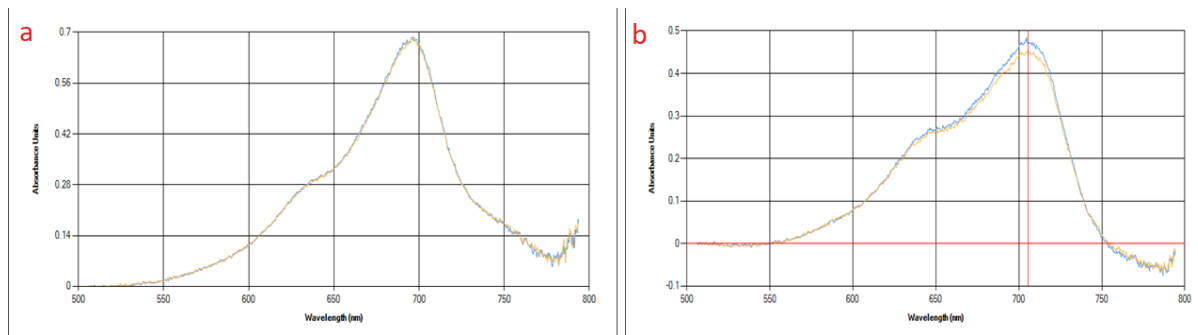


Figure 3.6 Reaction Initiation in SaBphP1-PCM-T289H Microcrystals. (a) Spectra of reaction initiation by laser. The blue line depicts the absorbance of the crystals after being adapted to the dark (Pr) state by a 740nm LED for 15 minutes. The gold line shows the absorbance after the microcrystals have been exposed to a single 660nm laser pulse. There is no change in the absorbance peak. (b) Spectra of reaction initiation by LED. The blue line depicts the absorbance of the crystals after being adapted to the dark (Pr) state by a 740 nm LED for 15 minutes. The gold line shows the absorbance after the microcrystals have been exposed to a 660nm LED for 15 minutes. There is a slight change in the central peak.

Tests were then done on the sample in solution to see if the inconsistency was due to crystallization. A single laser pulse failed to initiate the sample in solution as well. Activation of the solution with the 660nm LED showed the same inconsistency in the spectral change as in the microcrystals. A bleaching test was done with the laser to see if multiple laser pulses would have any effect on the sample in solution (Fig. 3.7a). Again, one laser pulse did not show any change, but multiple pulses show the same reduction of absorption across all peaks. Clearly after many pulses, this change is due to damage to the sample, but the early iterations still do not show the desired increase of absorption in the right-most peak.

The xenon light source that acts as the probe in the Schmidt Lab MSP has a spectral range between 350nm and 750nm. The right-most peak occurs around 750nm, at the very edge of the xenon light's wavelength range where the intensity drops off. As a result, the low intensity likely makes it difficult to calculate any change in spectra at this wavelength. This experiment would be better performed with a different light source that has a more appropriate wavelength range. A different spectrometer (a Thermo Scientific Evolution 60 Spectrophotometer) with a larger probing light wavelength range was used to confirm the

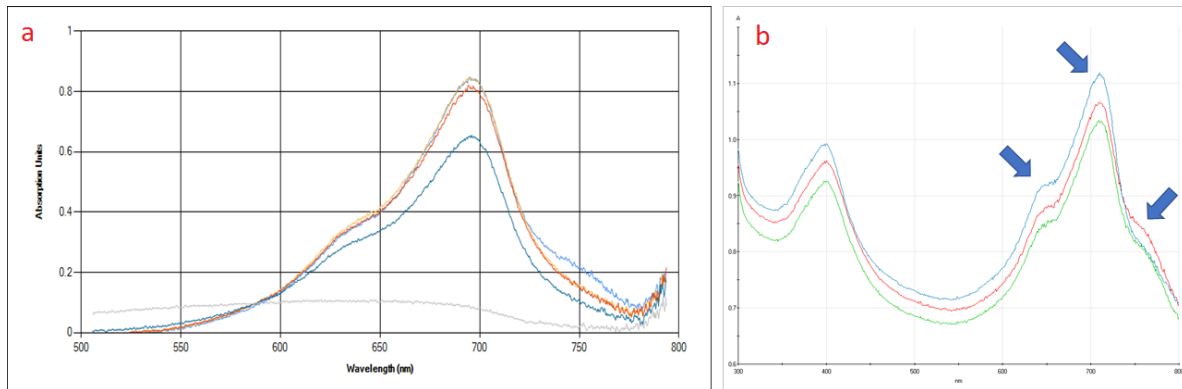


Figure 3.7 Laser Bleaching and Reaction Initiation Tests. (a) Spectra from bleaching of SaBphP1-PCM-T289H in solution due to multiple laser pulses. The light blue line depicts the absorbance of the solution after being adapted to the dark state (Pr) by a 740nm LED. The gold line was acquired after 1 laser pulse. The red line was acquired after 2 laser pulses. The dark blue line was acquired after 10 laser pulses. The grey line was acquired after 150 laser pulses and after an attempt to adapt the solution back to the dark (Pr) state by a 740nm LED for 15 minutes. (b) Spectra of reaction initiation of SaBphP1-PCM-T289H by LED captured on a Thermo Scientific Evolution 60 spectrophotometer. The blue line depicts the absorbance of the microcrystals after being adapted to the dark (Pr) state by a 740nm LED. The red line depicts the absorbance of the microcrystals after exposure to a 660nm LED. The left and central peaks show a decrease while the right peak shows an increase which is the expected reaction.

correct change in the absorption spectra for the microcrystals (Fig. 3.7b). While the Evolution spectrophotometer was able to confirm the correct spectral change, it is only capable of measuring a single spectrum from the protein after it has been exposed to light for a long time. The MSP can measure the spectral changes of the protein at specific time points during the reaction initiated by short laser pulses. These time-resolved spectra yield information about the process itself rather than simply confirming that it happened. For this reason, it is still important to continue these experiments on the MSP with a more suitable probing light wavelength range.

Introducing the T289H mutation causes structural displacements throughout the chromophore binding pocket. Adding on the PHY domain causes further displacements as well as a large effect on the relative orientation of the subunits when compared to SaBphP1. Thus, a better match is obtained by comparing SaBphP1-PCM-T289H to solved structures of BphPs which contain the PHY domain and the conserved His, like the *Deinococcus radiodurans* BphP

(DrBphP-PCM, solved in the Pfr state (Takala et al., 2014)) This comparison gives important insight into the nature of the switch between the Pr and Pfr states. In the Pr state, the tongue assumes a loop to β -sheet conformation while in the Pfr state it assumes a loop to α -helix conformation. An important proline residue is located in the sensory tongue (Pro-471). Normally, Pro destabilizes an α -helix because it disrupts the regularity of the α -helical backbone. However, a perturbation of Pro-471 by the Z-to-E isomerization of ring D of the chromophore (Fig. 3.4) allows for the transition to be completed. The helix conformation of the Pfr state causes the PHY domains to be pulled in opposite directions (Fig. 3.8). This movement also straightens out the kink in the helices which connect the GAF and PHY domains. The overall enzymatic activity of the output domain is largely affected by these conformational changes.

Performing a pump-probe laser excitation experiment with an XFEL provides the benefit of measuring the reaction as it happens at room temperature. We have seen an interesting

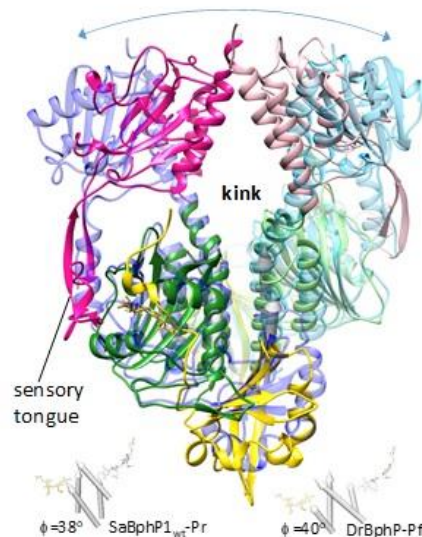


Figure 3.8 Models of PHY Domain During Pr-Pfr Switch. Overlaid structures of SaBphP1-PCM-T289H in the Pr state (PHY-yellow, GAF-green, and PHY-magenta) and DrBphP-PCM in the Pfr state (blue) as solved in (Takala et al., 2014). The blue arrow denotes the direction of the motion of the PHY domain during the switch. The kink, the point about which this motion pivots, is marked. The sensory tongue is marked. Below the structure, the four helices at the dimer interface are displayed as cylinders. This figure is adapted from (Woitowich et al., 2017) IUCrJ submitted.

difference in the Pr and Pfr states but the intermediate steps of the reaction must be further characterized. By performing the experiment again in vacuum to improve the resolution, an XFEL experiment is ideal for obtaining room temperature structures of these intermediates.

4 Conclusions and Outlook

The number of XFEL facilities in the world will continue to increase, with even more improved technology. XFELs at the LCLS-II and EuXFEL will provide pulses at rates on the order of MHz. Currently, we have shown that XFEL experiments are viable methods of obtaining macromolecular structures. In the future, these new facilities will be instrumental in obtaining room temperature structures of many important enzymatic processes and even single particles (Seibert et al., 2011).

Results of these MISC experiments (Chapter 3.1) show that it is possible to obtain structures of enzymatically catalyzed reactions on the order of milliseconds. MISC experiments enable the study of many non-cyclic reactions, which are more difficult to study without the serial nature of XFEL experiments. These reactions are important for further biological understanding, but some also are relevant targets in drug design. With faster pulse rates expected of future XFELs, capturing many more closely spaced time delays could lead to a more complete understanding of these reactions.

Recent TR-SFX experiments at LCLS (Pande et al., 2016; Tenboer et al., 2014) and SACLA (Nango et al., 2016) suggest that these experiments will also work for phytochromes. At SACLA,

the SaBphP1-PCM-T289H microcrystals scattered beyond 3Å in air (Chapter 3.2). This resolution could be improved by performing the experiment in vacuum. With a higher resolution possible, an important future goal is to determine the full-length structure of SaBphP1 including the histidine kinase output domain in both Pr and Pfr states. Beyond that, a similarly important goal would be to link the structural results to the observed photomorphogenic behavior.

5 References

- Adams, S. R., & Tsien, R. Y. (1993). CONTROLLING CELL CHEMISTRY WITH CAGED COMPOUNDS. *Annu. Rev. Physiol*, 55, 755–84. Retrieved from <http://www.annualreviews.org.ezproxy.lib.uwm.edu/doi/pdf/10.1146/annurev.ph.55.030193.003543>
- Auldridge, M. E., & Forest, K. T. (2011). Bacterial phytochromes: More than meets the light. *Critical Reviews in Biochemistry and Molecular Biology*, 46(1), 67–88. <https://doi.org/10.3109/10409238.2010.546389>
- Babic, M., Hujer, A. M., & Bonomo, R. A. (2006). What's new in antibiotic resistance? Focus on beta-lactamases. *Drug Resistance Updates*, 9, 142–156. <https://doi.org/10.1016/j.drug.2006.05.005>
- Bae, G., & Choi, G. (2008). Decoding of Light Signals by Plant Phytochromes and Their Interacting Proteins. *Annual Review of Plant Biology*, 59(1), 281–311. <https://doi.org/10.1146/annurev.arplant.59.032607.092859>
- Barty, A., Kirian, R. A., Maia, F. R. N. C., Hantke, M., Yoon, C. H., White, T. A., & Chapman, H. (2014). Cheetah: Software for high-throughput reduction and analysis of serial femtosecond X-ray diffraction data. *Journal of Applied Crystallography*, 47(3), 1118–1131. <https://doi.org/10.1107/S1600576714007626>
- Bhoo, S. H., Davis, S. J., Walker, J., Karniol, B., & Vierstra, R. D. (2001). Bacteriophytochromes are photochromic histidine kinases using a biliverdin chromophore. *Nature*, 414(6865), 776–779. <https://doi.org/10.1038/414776a>
- Bish, D. L., & Post, J. E. (1989). Modern powder diffraction. Washington, D.C.: Mineralogical Society of America. Retrieved from <http://catalog.hathitrust.org/api/volumes/oclc/20615367.html>
- Boutet, S., Lomb, L., Williams, G. J., Barends, T. R. M., Aquila, A., Doak, R. B., ... Schlichting, I. (2012). High-Resolution Protein Structure Determination by Serial Femtosecond Crystallography. *Science*, 337(6092), 362–364. <https://doi.org/10.1126/science.1217737>
- Boyd, D. B., Herron, D. K., Lunn, W. H. W., & Spitzer, W. A. (1980). Parabolic Relationships between Antibacterial Activity of Cephalosporins and P-Lactam Reactivity Predicted from Molecular Orbital Calculations'. *Journal of the American Chemical Society*, 1026. Retrieved from <http://pubs.acs.org.ezproxy.lib.uwm.edu/doi/pdf/10.1021/ja00526a009>
- Burgie, E. S., Wang, T., Bussell, A. N., Walker, J. M., Li, H., & Vierstra, R. D. (2014). Crystallographic and electron microscopic analyses of a bacterial phytochrome reveal local and global rearrangements during photoconversion. *Journal of Biological Chemistry*, 289(35), 24573–24587. <https://doi.org/10.1074/jbc.M114.571661>
- Bush, K., & Fisher, J. F. (2011). Epidemiological Expansion, Structural Studies, and Clinical

- Challenges of New β -Lactamases from Gram-Negative Bacteria. *Annual Review of Microbiology*, 65(1), 455–478. <https://doi.org/10.1146/annurev-micro-090110-102911>
- Calvey, G. D., Katz, A. M., Schaffer, C. B., & Pollack, L. (2016). Mixing injector enables time-resolved crystallography with high hit rate at X-ray free electron lasers. *Structural Dynamics*, 3(5). <https://doi.org/10.1063/1.4961971>
- Cartlidge, E. (2016). European XFEL to shine as brightest, fastest x-ray source. *Science*, 354(6308), 22–23. <https://doi.org/10.1126/science.354.6308.22>
- Chantemesse, B., Betelli, L., Solanas, S., Vienney, F., Bollache, L., Hartmann, A., & Rochelet, M. (2017). A nitrocefin-based amperometric assay for the rapid quantification of extended-spectrum β -lactamase-producing *Escherichia coli* in wastewaters. *Water Research*, 109, 375–381. <https://doi.org/10.1016/j.watres.2016.11.066>
- Chapman, B. M., & Massaioli, F. (2005, October 1). OpenMP. *Parallel Computing*, 31(10–12), 957–959. <https://doi.org/10.1016/j.parco.2005.08.001>
- Cho, H. S., Dashdorj, N., Schotte, F., Graber, T., Henning, R., & Anfinrud, P. (2010). Protein structural dynamics in solution unveiled via 100-ps time-resolved x-ray scattering. *Proceedings of the National Academy of Sciences of the United States of America*, 107(16), 7281–6. <https://doi.org/10.1073/pnas.1002951107>
- Chow, C., Xu, H., & Blanchard, J. S. (2013). Kinetic characterization of hydrolysis of nitrocefin, cefoxitin, and meropenem by β -lactamase from mycobacterium tuberculosis. *Biochemistry*, 52(23), 4097–4104. <https://doi.org/10.1021/bi400177y>
- Dubée, V., Triboulet, S., Mainardi, J. L., Ethève-Quellejeu, M., Gutmann, L., Marie, A., ... Arthur, M. (2012). Inactivation of Mycobacterium tuberculosis L,D-transpeptidase Ldt Mt1 by carbapenems and cephalosporins. *Antimicrobial Agents and Chemotherapy*, 56(8), 4189–4195. <https://doi.org/10.1128/AAC.00665-12>
- Edlund, P., Takala, H., Claesson, E., Henry, L., Dods, R., Lehtivuori, H., ... Westenhoff, S. (2016). The room temperature crystal structure of a bacterial phytochrome determined by serial femtosecond crystallography. *Scientific Reports*, 6(May), 1–9. <https://doi.org/10.1038/srep35279>
- Emma, P., Akre, R., Arthur, J., Bionta, R., Bostedt, C., Bozek, J., ... Galayda, J. (2010). First lasing and operation of an ångström-wavelength free-electron laser. *Nature Photonics*, 4(9), 641–647. <https://doi.org/10.1038/nphoton.2010.176>
- Gan, F., Zhang, S., Rockwell, N. C., Martin, S. S., Lagarias, J. C., & Bryant, D. A. (2014). Extensive remodeling of a cyanobacterial photosynthetic apparatus in far-red light. *Science*, 345(6202), 1312–1317. <https://doi.org/10.1126/science.1256963>
- Graber, T., Anderson, S., Brewer, H., Chen, Y.-S., Cho, H. S., Dashdorj, N., ... Moffat, K. (2011). BioCARS: a synchrotron resource for time-resolved X-ray science. *Journal of Synchrotron Radiation*, 18(4), 658–670. <https://doi.org/10.1107/S0909049511009423>

- Hughes, J. (2013). Phytochrome Cytoplasmic Signaling. *Annual Review of Plant Biology*, 64(1), 377–402. <https://doi.org/10.1146/annurev-arplant-050312-120045>
- Hughes, J., Lamparter, T., Mittmann, F., Hartmann, E., Gärtner, W., Wilde, A., & Börner, T. (1997). A prokaryotic phytochrome. *Nature*, 386(6626), 663–663. <https://doi.org/10.1038/386663a0>
- Hugonnet, J.-E., & Blanchard, J. S. (2007). Irreversible inhibition of the Mycobacterium tuberculosis beta-lactamase by clavulanate. *Biochemistry*, 46(43), 11998–12004. <https://doi.org/10.1021/bi701506h.Irreversible>
- Hugonnet, J.-E., Tremblay, L. W., Boshoff, H. I., Barry, C. E., & Blanchard, J. S. (2009). Meropenem-Clavulanate Is Effective Against Extensively Drug-Resistant Mycobacterium tuberculosis. *Science*, 323(5918), 1215–1218. <https://doi.org/10.1126/science.1167498>
- Jeon, J. H., Lee, J. H., Lee, J. J., Park, K. S., Karim, A. M., Lee, C. R., ... Lee, S. H. (2015). Structural basis for carbapenem-hydrolyzing mechanisms of carbapenemases conferring antibiotic resistance. *International Journal of Molecular Sciences*, 16(5), 9654–9692. <https://doi.org/10.3390/ijms16059654>
- Kameshima, T., Ono, S., Kudo, T., Ozaki, K., Kirihara, Y., Kobayashi, K., ... Hatsui, T. (2014). Development of an X-ray pixel detector with multi-port charge-coupled device for X-ray free-electron laser experiments. *Citation: Review of Scientific Instruments*, 85(33110). Retrieved from <https://doi.org/10.1063/1.4867668>
- Kato, M., Tanaka, T., Kurosawa, T., Saito, N., Richter, M., Sorokin, A. A., ... Ishikawa, T. (2012). Pulse energy measurement at the hard x-ray laser in Japan. *Applied Physics Letters*, 101(2). <https://doi.org/10.1063/1.4733354>
- Kupitz, C., Olmos, J. L., Holl, M., Tremblay, L., Pande, K., Pandey, S., ... Schmidt, M. (2017). Structural enzymology using X-ray free electron lasers. *Structural Dynamics*, 4(4). <https://doi.org/10.1063/1.4972069>
- Lagarias, J. C., & Rapoport, H. (1980). Chromopeptides from Phytochrome. The Structure and Linkage of the PRForm of the Phytochrome Chromophore. *Journal of the American Chemical Society*, 102(14), 4821–4828. <https://doi.org/10.1021/ja00534a042>
- Liang, M., Williams, G. J., Messerschmidt, M., Seibert, M. M., Montanez, P. A., Hayes, M., ... Boutet, S. (2015). The Coherent X-ray Imaging instrument at the Linac Coherent Light Source. *J. Synchrotron Rad*, 22, 514–519. <https://doi.org/10.1107/S160057751500449X>
- Nakane, T., Joti, Y., Tono, K., Yabashi, M., Nango, E., Iwata, S., ... Nureki, O. (2016). Data processing pipeline for serial femtosecond crystallography at SACLA. *Journal of Applied Crystallography*, 49, 1035–1041. <https://doi.org/10.1107/S1600576716005720>
- Nango, E., Royant, A., Kubo, M., Nakane, T., Wickstrand, C., Kimura, T., ... Iwata, S. (2016). A three-dimensional movie of structural changes in bacteriorhodopsin. *Science*, 354(6319), 1552–1557. <https://doi.org/10.1126/science.aah3497>

- Neutze, R., Wouts, R., van der Spoel, D., Weckert, E., & Hajdu, J. (2000). Potential for biomolecular imaging with femtosecond X-ray pulses. *Nature*, *406*(6797), 752–757. <https://doi.org/10.1038/35021099>
- Pande, K., Hutchison, C. D. M., Groenhof, G., Aquila, A., Robinson, J. S., Tenboer, J., ... Schmidt, M. (2016). Femtosecond structural dynamics drives the trans/cis isomerization in photoactive yellow protein. *Science*, *352*(6286), 725–729. <https://doi.org/10.1126/science.aad5081>
- Pile, D. (2011). X-rays: First light from SACLA. <https://doi.org/10.1038/nphoton.2011.178>
- Purwar, N., Tenboer, J., Tripathi, S., & Schmidt, M. (2013). Spectroscopic studies of model photo-receptors: Validation of a nanosecond time-resolved micro-spectrophotometer design using photoactive yellow protein and ??-phycoerythrocyanin. *International Journal of Molecular Sciences*, *14*(9), 18881–18898. <https://doi.org/10.3390/ijms140918881>
- Schmidt, M. (2013). Mix and inject: Reaction initiation by diffusion for time-resolved macromolecular crystallography. *Advances in Condensed Matter Physics*, *2013*. <https://doi.org/10.1155/2013/167276>
- Schotte, F. (2003). Watching a Protein as it Functions with 150-ps Time-Resolved X-ray Crystallography. *Science*, *300*(5627), 1944–1947. <https://doi.org/10.1126/science.1078797>
- Seibert, M. M., Ekeberg, T., Maia, F. R. N. C., Svenda, M., Andreasson, J., Jönsson, O., ... Hajdu, J. (2011). Single mimivirus particles intercepted and imaged with an X-ray laser. *Nature*, *470*(7332), 78–82. <https://doi.org/10.1038/nature09748>
- Takala, H., Björling, A., Berntsson, O., Lehtivuori, H., Niebling, S., Hoernke, M., ... Westenhoff, S. (2014). Signal amplification and transduction in phytochrome photosensors. *Nature*, *509*(7499), 245–248. <https://doi.org/10.1038/nature13310>
- Tasler, R., Moises, T., & Frankenberg-Dinkel, N. (2005). Biochemical and spectroscopic characterization of the bacterial phytochrome of *Pseudomonas aeruginosa*. *FEBS Journal*, *272*(8), 1927–1936. <https://doi.org/10.1111/j.1742-4658.2005.04623.x>
- Tenboer, J., Basu, S., Zatsepin, N., Pande, K., Milathianaki, D., Frank, M., ... Schmidt, M. (2014). Time-resolved serial crystallography captures high-resolution intermediates of photoactive yellow protein. *Science*, *346*(6214), 1242–1246. <https://doi.org/10.1126/science.1259357>
- Tremblay, L. W., Fan, F., & Blanchard, J. S. (2010). Biochemical and structural characterization of mycobacterium tuberculosis ??-lactamase with the carbapenems ertapenem and doripenem. *Biochemistry*, *49*(17), 3766–3773. <https://doi.org/10.1021/bi100232q>
- Tukey, J. W. (1977). *Exploratory data analysis*. Reading, Mass.: Addison-Wesley Pub. Co.
- Ursby, T., Weik, M., Fioravanti, E., Delarue, M., Goeldner, M., & Bourgeois, D. (2002). Cryophotolysis of caged compounds: a technique for trapping intermediate states in protein crystals. *Acta Crystallographica Section D Biological Crystallography*, *58*(4), 607–614. <https://doi.org/10.1107/S0907444902002135>

- Voladri, R. K., Lakey, D. L., Hennigan, S. H., Menzies, B. E., Edwards, K. M., & Kernodle, D. S. (1998). Recombinant expression and characterization of the major β -lactamase of *Mycobacterium tuberculosis*. *Antimicrobial Agents and Chemotherapy*, 42(6), 1375–1381.
- Wang, F., Cassidy, C., & Sacchettini, J. C. (2006). Crystal structure and activity studies of the *Mycobacterium tuberculosis* β -lactamase reveal its critical role in resistance to β -lactam antibiotics. *Antimicrobial Agents and Chemotherapy*, 50(8), 2762–2771.
<https://doi.org/10.1128/AAC.00320-06>
- White, T. A., Mariani, V., Brehm, W., Yefanov, O., Barty, A., Beyerlein, K. R., ... Chapman, H. N. (2016). Recent developments in CrystFEL. *Journal of Applied Crystallography*, 49, 680–689.
<https://doi.org/10.1107/S1600576716004751>
- White, W. E., Robert, A., & Dunne, M. (2015). The linac coherent light source. *Journal of Synchrotron Radiation*, 22(October 2009), 472–476.
<https://doi.org/10.1107/S1600577515005196>
- WHO. (2016). Global Tuberculosis Report 2016. *Cdc 2016*, (Global TB Report 2016), 214.
<https://doi.org/ISBN 978 92 4 156539 4>
- Winn, M. D., Ballard, C. C., Cowtan, K. D., Dodson, E. J., Emsley, P., Evans, P. R., ... Wilson, K. S. (2011). Overview of the CCP4 suite and current developments. *Acta Crystallographica Section D: Biological Crystallography*, 67(4), 235–242.
<https://doi.org/10.1107/S0907444910045749>

Appendix A: MAX-302 Xenon Light Source

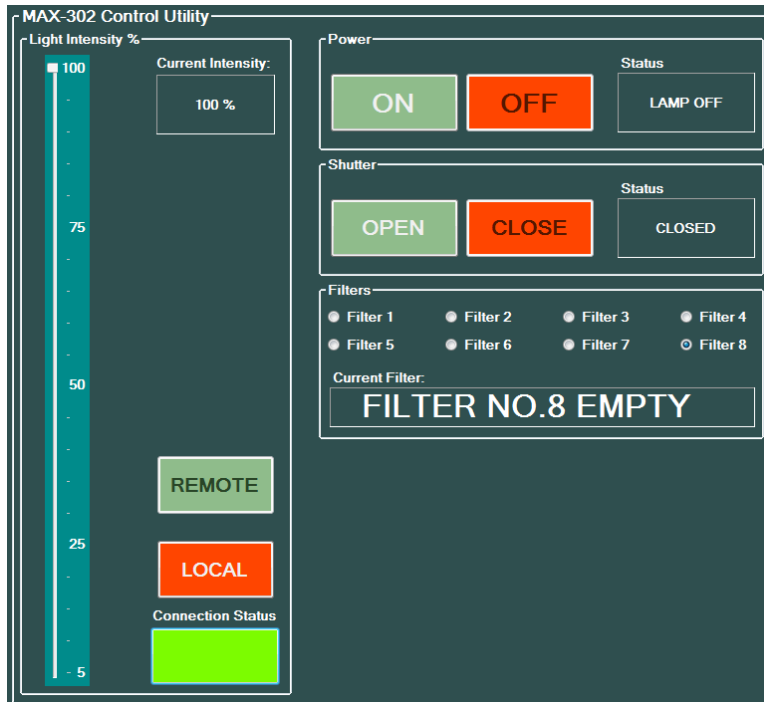


Figure A.1 GOEGUI – Max-302 Control Utility. The figure depicts the program after the connection has been made.

The MAX-302 has one straight-forward but important function: to produce continuous-wave white light. The machine has other features to augment the light but they are not used very often as the full intensity of the light is typically used for spectra experiments. These features include: an internal shutter to block or allow all light, filters to block or allow certain portions of light, and the ability to change the intensity of the light. The MAX-302 can be controlled using the buttons on the machine itself, but using a GUI is more user-friendly. The GUI separates the controls for different functions into appropriate Groupboxes for ease of use. The following will describe how to control the machine using the GUI which was mainly developed by myself (Fig. A.1). Instructions to operate the MAX-302 manually are found in the MAX-302 User Manual.

Lamp

The power switch is located on the back of the MAX-302. The MAX-302 must be powered on before a connection can be made through the GUI. Connection to the MAX-302 is achieved by clicking the connect button. In GOEGUI, the connect button is under the connections tab, but clicking the Connection Status button under the MAX-302 tab will also make the connection. Once the connection is made, the MAX-302 will automatically be put in remote mode and the buttons on the MAX-302 will not work. Switching between remote and local modes is achieved by clicking their respective buttons. The lamp is controlled by the On and Off buttons in the Power Groupbox.

The lamp should not be turned on and off multiple times in a short period (referred to as cycling the lamp) as this can damage the lamp. When the lamp is turned off, the machine should be left on for about 15 minutes (or until the fan exhaust runs cool) to allow the lamp to cool down. A pop-up message will show a reminder for these issues every time the lamp is turned off.

The lamp will eventually need to be changed when it reaches the end of its lifetime. The lamp hours can be checked using the buttons on the machine. (A GUI interface is possible for this, but was not included due to rarity of use.) The current lamp was installed when the lamp hours read: 1366 hours. The manual contains specifics regarding lamp lifetime and replacement.

Light Intensity

Intensity of the light is controlled by using the slider bar in the Light Intensity Groupbox. The minimum light intensity is 5%. To achieve 0% light intensity a shutter must be closed. Typically, 100% light intensity is used for experiments, but it can be helpful to lower the intensity for alignment purposes.

Internal Shutter

The MAX-302 Internal Shutter is controlled by the Open and Close buttons in the Shutter Groupbox. Since there is an external Thorlabs' Shutter which controls admittance of light from the MAX-302 to the sample stage, there is no reason for the internal shutter to be closed while using the MAX-302. However, the shutter should be closed each time the machine is turned off. The lamp will not turn on if the internal shutter is open. The lamp should always be turned on first, and the shutter opened after.

Filters

The MAX-302 houses a filter wheel which holds 8 different filters. Selecting a filter is done by clicking one of the radio buttons in the Filters Groupbox. Typically, filter 8 is used since it is empty and the program selects it by default. A list of the current filters installed in the filter wheel is provided in Table A1.

Table A.1 Max-302 Filters. The current filters installed in the filter wheel are listed here.

Filter 1	OD: 0.2
Filter 2	OD: 0.5
Filter 3	OD: 1.0
Filter 4	OD: 4.0
Filter 5	OD: 6.0
Filter 6	EMPTY
Filter 7	EMPTY
Filter 8	EMPTY

Appendix B: Opolette Nanosecond Laser

The Opolette Laser is used as the pump in spectroscopic pump-probe experiments. It is a class 4 laser which is capable of severe injury so extreme care must be taken to avoid laser exposure to the eyes especially, but also to the rest of the body. The Schmidt lab has two types of protective laser goggles. The correct type of goggles for the laser wavelength being used must be worn while operating the laser. The Optical Density (OD) at different wavelengths is printed on both types of goggles. The goggles with the highest OD for the wavelength being used should be worn. If neither of the goggles have a high OD for the wavelength being used, new goggles for that wavelength must be acquired. Inadequate goggles should not be used under the assumption that they will provide appropriate protection. Additionally, care should be taken to avoid looking out the sides of the goggles. While the laser should be contained to a certain path, it is possible for the laser to reflect on the many metal surfaces in the table. The laser setup has a few different parts.

ICE450

The ICE450 pumps water to the laser head to cool it down. It is turned on with a key on its front. Occasionally, the water will have to be refilled. The system will issue a warning when a refill is necessary. If the laser is to be shipped somewhere, it will be necessary to completely empty the water from the lines so they do not freeze in a plane's cargo hold. Information on filling or emptying the water is in the ICE450 User Manual.

Electronics Box

The Electronics Box facilitates communication between the laser and the computer. It only has a power switch and just needs to be turned on before the laser control software can be used.

Laser Control Software

Upon opening the Control Software (Fig. B.1), which is provided by Oportek, the laser motors will align themselves. Once this is finished, the controls will show up. The following instructions are for the controls currently most often used. The laser's other features are described in the Opolette 355 User Manual.

The flashlamp is activated by pressing the LAMP button. The software will count down 10 seconds until the laser is available. Currently, the flashlamp actually takes about 2 hours to warm up, and the laser reaches full laser power.

Once the flashlamp is on, two more buttons will appear below the LAMP button. Pressing LASER will turn the Q-switch on and the laser will start firing with the selected Energy, Rep Rate, and Wavelength until the LASER Button is pressed again. Pressing 1-SHOT will fire just one laser pulse with the selected Energy, Rep Rate, and Wavelength.

The laser energy can be adjusted with either the slider bar or the text box located under 'Energy (%)'. Typically, this will be set to 100% for all experiment purposes, however, it may need to be lowered for alignment purposes. The program always initializes the laser energy to 0% and it must be adjusted on start-up every time.

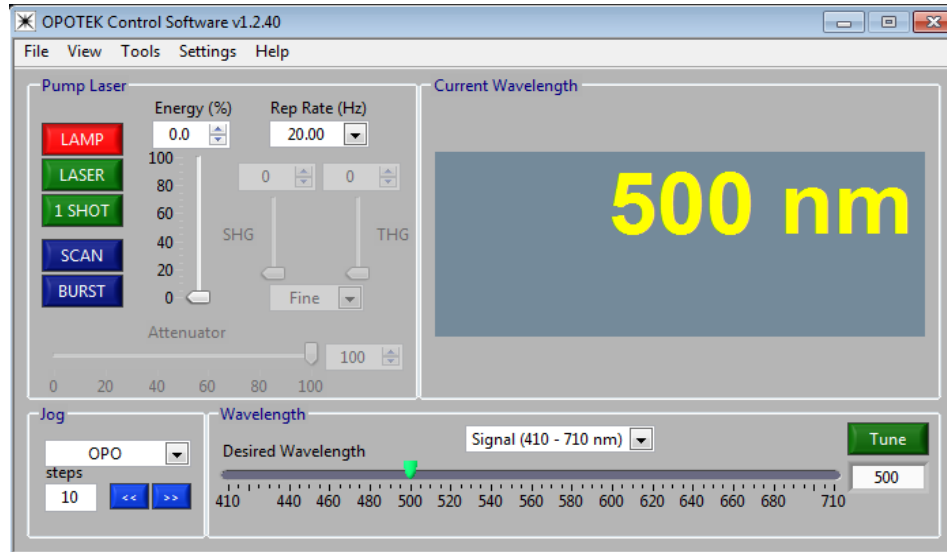


Figure B.1 OPOTEK Laser Control Software. The figure depicts the software after the flashlamp has been turned on.

The repetition rate can be adjusted with the text box located under 'Rep Rate (Hz)'. Typically, this will be set to 20 Hz for all experiment purposes.

The laser wavelength can be tuned with the slider bar located in the Wavelength Groupbox, but it is far easier to type the desired wavelength into the text box to the right and then press the Tune Button. The software will pause while the laser tunes in the specified wavelength.

Remote Control

Once the flashlamp is on, the Q-switch can be triggered by the remote control. This can be useful for quick laser tests when aligning the laser. The remote control is also the only place to set the Q-switch trigger source. By default, the trigger source is set to external whenever the machine is turned on, which means it must be set to internal before the remote control or even the buttons on the control software will produce a laser beam, as the machine will be waiting for an external source before actually firing the laser. The option to change the trigger source is

located under Main Menu >> Q-Switch >> QS sync: INT/EXT on the remote control. During an experiment, the Q-switch will be controlled by the DG645 as an external source and so when doing experiments, the Q-switch trigger source must be set to external.

Appendix C: Shutters



Figure C.1 GOEGUI – ThorLabs Shutter Control Utility. The figure depicts the program after the connection has been made.

There are 2 Thor Labs shutters utilized in the MSP: one that blocks the Opolette Laser beam (Laser Shutter) and one that blocks the MAX-302 light beam (Xenon Shutter). The Laser Shutter is located just in front of the Opolette Laser inside of the laser optics box. The Xenon Shutter is located inside the MAX-302 optics box. The shutters have a few features, but they are mostly used manually to block or allow the light when desired, in addition to safety purposes for the Laser Shutter.

Both shutters can be operated under the same tab in GOEGUI (Fig. C.1). The shutters can be opened and closed by clicking the Enable/Disable button in the Controls Groupbox. It is also possible to manually press the Enable button on the shutter controller. Pressing this button

manually is often quicker than accessing the GUI. Switching between internal and external triggers is done by clicking the External/Internal button under 'Set Trigger Source' in the Controls Groupbox. The Shutter Mode (Tab. C.1) can be set by selecting a mode from the Set Mode Menubox in the Controls Groupbox.

Table C.1 ThorLabs Shutter Modes. A description of the different shutter modes that can be set in the Set Mode Menubox.

Manual	The shutter will open when Enable is pressed and close when Disable is pressed.
Single	The shutter will open when Enable is pressed and close after the specified Shutter Open Time.
Repeat	The shutter will open when Enable is pressed and close after the specified Shutter Open Time. After the specified Shutter Close Time, the shutter will open again. The shutter will open and close the number of times specified by Repetition Count.
Auto	The shutter will open when Enable is pressed and close after the specified Shutter Open Time. After the specified Shutter Close Time, the shutter will open again. The shutter will open and close indefinitely until Disable is pressed.
X Gate	External Gate Mode. The shutter will open and close according to external trigger pulses from a device connected to the shutter controller (likely a Digital Delay Generator). This mode differs from simply setting the trigger source to external in that this mode will open and close only when the external device signals. Setting the trigger source to external will cause the shutter to undergo its specified Mode, Open Time, Close Time, and Repetitions when the external device signals.

Currently, when taking spectra, the Andor SOLIS program will open its own COM port connection to the shutter controllers and send the signal to open and close on its own. For this reason, the shutters will only need to be turned on and left in manual mode. Further information on these features is contained in the ThorLabs Shutter Controller User Manual.

Appendix D: Fiber-Coupled LED

LEDs are used to reset the conformation of proteins to the same initial state after laser/light exposure. There are 2 main parts to the LED setup.

T-Cube LED Driver

The LED Driver has a dial which controls the LED brightness and a switch that sets the 3 possible modes: CW, TRIG, and MOD (Tab. D.1). Currently, the LED is only controlled manually in CW Mode. If the LED is to be used with the DDG, it will need to be set to Trigger Mode.

Table D.1 LED Driver Modes. A description of the different driver modes that can be set on the T-Cube LED driver.

CW	Constant Continuous Wave Light.
TRIG	Trigger Mode. Allows an external source to turn the LED on or off. Brightness will be set by the dial.
MOD	Modulation Mode. Allows an external source to control the LED completely, turning it on or off as well as modulate the brightness.

Individual LED Modules

There is a different module for each wavelength of LED. Specific information for each module can be found on the ThorLabs website. The lab currently has the following LED wavelengths: 470nm, 490nm, 590nm, 660nm, 740nm.

Each module has an attached cable which connects to the LED Driver. Each should be labelled with an Amperage. There is a dial on the side of the LED Driver which must be set to the amperage for the module that is being attached. It is important to change the driver to the correct amperage for each module to avoid damage to the LED. If a module is not labelled with its amperage, it can be found on the ThorLabs site.

The module must also be connected to the red optical fiber which carries the LED to the sample stage. Each module has a red cap that protects this connector. The cap needs to be replaced after removing the optical fiber from a module to prevent damage to the LED.

Appendix E: DG645 Digital Delay Generator

The DG645 is a Digital Delay Generator (DDG) which connects some of the machines in the MSP together. The DDG sends out pulses at specific times in order to facilitate the timing of the machines' functions with respect to one another.

DG645 Digital Delay Generator Control Utility				
Status				
Channel	W.R.T. Channel	Delay	Amplitude	Polarity
T1	T0	+3.00000025000 sec	+5.00 volts	POSITIVE
A	T0	+0.00000000000 sec	+5.00 volts	POSITIVE
B	A	+0.00000000000 sec	+5.00 volts	POSITIVE
C	T0	+1.00000000000 sec	+5.00 volts	POSITIVE
D	C	+2.00000000000 sec	+5.00 volts	POSITIVE
E	T0	+0.00000000000 sec	+5.00 volts	POSITIVE
F	E	+0.00000000000 sec	+5.00 volts	POSITIVE
G	F	+0.00000000000 sec	+5.00 volts	POSITIVE
H	G	+0.00000000000 sec	+5.00 volts	POSITIVE

Controls				
Channel	W.R.T. Channel	Delay	Amplitude	Polarity
T1	Automatic	Automatic	Format: n.nn	POS
A	T0	Format: seconds	Format: n.nn	POS
B	A	Format: seconds	Same as A	Same as A
C	T0	Format: seconds	Format: n.nn	POS
D	C	Format: seconds	Same as C	Same as C
E	T0	Format: seconds	Format: n.nn	POS
F	E	Format: seconds	Same as E	Same as E
G	F	Format: seconds	Format: n.nn	POS
H	G	Format: seconds	Same as G	Same as G

Figure E.1 GOEGUI – DG645 Digital Delay Generator Control Utility. The figure depicts the program after the connection has been made.

The DDG has 10 channels: T0, T1, A, B, C, D, E, F, G, H. Each of these channels can be set with respect to another channel with a delay indicating how much time occurs between each point (Fig E.1). Each pairing of channels creates a pulse with each channel being an endpoint of the pulse. The delay for the first channel indicates when the pulse begins and the delay for the second channel indicates how long the pulse lasts. These pulses then trigger different machines

in the MSP to activate/deactivate with the same separation in time every time the DDG executes the series of pulses.

Channel T0 is the reference channel which marks the beginning of the main pulse. Channel T1 is the end channel which marks the end of the main pulse. It is automatically set with respect to channel T0 with a delay which is 25 nanoseconds after the end of the last sub-pulse. Each of the channel pairs A, B; C, D; E, F; G, H form a pulse.

Typically, the first channel will be set with respect to T0 meaning the delay indicates how long after the main pulse that the associated sub-pulse begins. The second channel will be set with respect to the first channel, meaning the delay indicates how long the pulse will last. Of course, they need not be set this way. The DDG controls are fairly flexible and should accommodate whichever way it makes the most sense to set the channels with respect to one another.

The DDG can be set to run the series of pulses internally or to be triggered by an external source. When an experiment is running, the DDG will be set to an external trigger source and will be triggered by the Q-switch. The program which runs the experiment sets the DDG timing so that the laser pulse, which arrives a certain time after the Q-switch pulse, arrives at just the right time with respect to all of the other machines' functions. More information on the timing of the spectroscopic experiment are described in Spectroscopic Studies of Model Photo-Receptors (Purwar et al., 2013)

Appendix F: Andor SOLIS, Shamrock and iStar

The Andor Shamrock spectrometer and iStar camera are mainly operated through the Andor SOLIS program. GOEGUI can change the machine settings but cannot take data. There is no manual interface for these machines; all communication is through the computer.

Upon opening SOLIS, the program will connect to the Shamrock and iStar. The iStar and Shamrock must be powered on in order to connect. The iStar will always be powered on as long as it is plugged in, but the Shamrock has a power unit that must be switched on. The iStar and Shamrock are not Hot-Pluggable, that is, they should not be connected or disconnected while the host computer is on. Doing so can damage detector circuitry.

The iStar camera maintains a low temperature for the CCD using a cooler. The cooler set point is set to -20° Celsius and will automatically turn on when the program connects. Spectra should only be taken after the set point is reached. The temperature is displayed in the bottom left corner of SOLIS.

Shamrock Settings

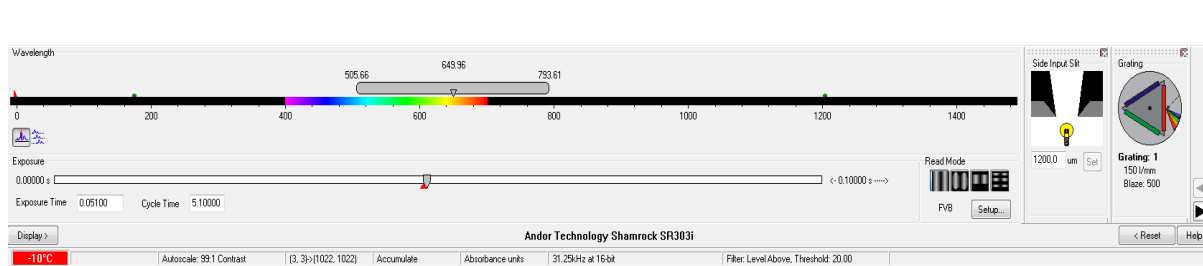


Figure F.1 Andor SOLIS – Shamrock Display Bar. This display will appear upon successful connection to the Shamrock spectrometer.

A display for the Shamrock spectrometer should appear at the bottom of SOLIS once the program connects (Fig. F.1). The following settings can be set using this interface.

Grating

Three diffraction gratings are installed in the Shamrock. They have the following lines/mm: 150, 599, 1199. Each grating has a different range of wavelengths that it can read. Grating 1 (150 Lines/mm) has the largest range, followed by Grating 2 (599 Lines/mm), and lastly Grating 3 (1199 Lines/mm) which has the smallest range. Typically, Grating 1 is used for its larger wavelength range, but it lacks the ability to see finer details in the spectra. To see finer detail, Grating 3 can be used and the range can be gained back by using the step-and-glue function (explained below).

Slit Width

The width of the slit through which the light is delivered can be adjusted. Typically, it is left at its largest width to let in all of the light.

Wavelength

The gratings can only read a range of wavelengths, but that range can be adjusted using the wavelength slider bar. The center wavelength as well as the endpoints of the range are shown above the bar. The locations of the visible light wavelengths are shown on the bar as well.

Step-and-Glue

Just below the wavelength slider bar are two buttons which switches between two modes, Wavedrive (normal) and Step-and-Glue. Step-and-Glue takes many spectra over a certain range and pastes them together with a certain amount of overlap. This is usually done

with Grating 3 and creates a spectrum with both range and fine detail. This is mostly used for aligning the spectrometer using the Ocean Optics Calibration Source. A spectrum must be obtained that spans a large wavelength range but also captures some of the smaller peaks produced by the source.

iStar Settings

Some of the iStar settings appear beneath the Shamrock Display, but for the most part, they are found in the Menu Bar under Acquisition. Going to Acquisition >> Setup Acquisition yields a pop-up window where the iStar settings are found (Fig. F.2). The most used settings are described. Other settings, as well as the full details of all settings, are described in the Andor iStar User Manual.

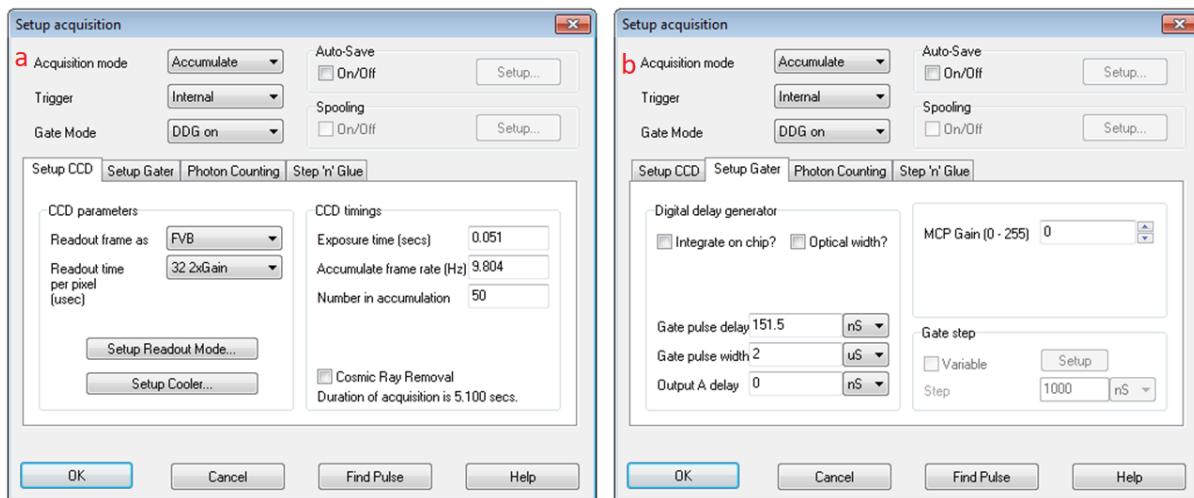


Figure F.2 Andor SOLIS – Setup Acquisition. (a) Setup CCD Tab. (b) Setup Gater Tab.

Acquisition Mode

The acquisition mode sets the type of spectrum collection to run. The most used are Single Scan, Accumulate, and Real Time (Tab. F.1). The Kinetic Series and Fast Kinetics modes are described in the Andor iStar User Manual.

Table F.1 iStar Acquisition Modes. A description of the Acquisition Modes that can be set in the Setup Acquisition Menu.

Single Scan	Takes a single spectrum.
Accumulate	Takes a specified number of spectra and averages them into one. Useful for obtaining cleaner spectra as averaging smooths out variations often present in a single spectrum.
Real Time	Shows the real-time display of the light on the CCD. Necessary for alignment. To use, 'Readout Frame' must be set to 'Image' and 'Readout Time per pixel' must be set to '1'.

Trigger

The trigger source for the camera can be set to Internal or External. In this drop-down menu, the trigger will usually be Internal by default. For a laser experiment, the trigger source will be set to external elsewhere by a program.

Under the Setup CCD Tab

The right side of this tab will contain different settings depending on the chosen Acquisition Mode (Fig. F.2a). The CCD parameters are described in Table F.2.

Table F.2 Setup Acquisition – Setup CCD Tab. A description of the CCD settings that can be set in the Setup Acquisition Menu.

CCD Parameters	
Readout Frame as	Typically set to FVB (Full Vertical Binning). Must be set to Image in order to use Real Time for alignment.
Readout Time per pixel	Typically set to 32 (2x Gain). Must be set to 1 in order to use Real Time for alignment.
CCD Timings	
Exposure Time [all]	Usually set to the minimum value. (Depends on other settings, enter zero to automatically calculate minimum value.)
Accumulate Frame Rate [Accumulate]	Usually set to the maximum value. (Depends on other settings, enter a large number to calculate the maximum value.)
Number in Accumulation [Accumulate]	The desired number of images to accumulate.
Frame Rate [Real Time]	Usually set to the maximum value. (Max frame rate is 9.804 Hz).

Under the Setup Gater Tab

The iStar has an internal digital delay generator which can shape the timing and length of the pulse which tells the camera to collect data. The parameters which shape this pulse are found under the Setup Gater tab (Fig. F.2b) and described in Table F.3.

Data Type

Going to Acquisition >> Setup Data Type yields a pop-up box where the data type can be set. There are many options, but most are not used. Absorbance Units are always used for experiment. Sometimes, it may be necessary to use the basic type Counts.

Table F.3 Setup Acquisition – Setup Gater Tab. A description of the Gating settings that can be set in the Setup Acquisition Menu.

Digital Delay Generator	
Gate Pulse Delay	Determines how long after the start of acquisition the pulse begins. Usually set to the (experimentally determined) time that the peak of the laser pulse hits the sample. This is so that non-laser spectra can be used as tests with similar settings before actually running the laser experiment.
Gate Pulse Width	Width of the pulse. Determines time resolution of the experiment. Should be in the same range as the time-point being measured.
Output A Delay	Defines a delay for a pulse that is sent out to another piece of equipment by the iStar. Not currently used, typically set to 0.
MCP Gain	
MCP Gain	Using an MCP Gain can increase the signal of a spectra. If the signal does not have a high enough absorbance, use MCP gain to get a better signal.

Appendix G: iStar Acquisition Types

Table G.1 iStar Acquisition Types. A description of the different Acquisition Types that are used in the process of taking spectra.

Background	Data collected with no light falling onto the CCD. Subtracted from the final signal to remove background noise from the image. Taken with Acquisition >> Take Background >> Photo-Cathode Off or [Ctrl+B].
Reference	Most samples will be sitting in solution inside some kind of glass apparatus, both of which will contribute their own absorbance. Reference data is collected by shining light through just the solution in the apparatus. The extra absorbance is then subtracted from the final signal to get a more accurate image of the sample's absorbance. Taken with Acquisition >> Take Reference or [Ctrl+R].
Signal	Data collected with light shining on the sample. Taken with Acquisition >> Take Signal or [F5].

Appendix H: Procedure for Taking Single Spectra

Table H.1 Procedure for Taking Single Spectra. A general description of the procedure for taking single spectra.

1. Setup Acquisition	Most of the parameters can stay the same, but the values should be verified before the program starts. The usual ones to change are Acquisition Mode (Single Scan or Accumulate are possible) or MCP Gain.
2. Align Reference Solution	The sample buffer should be aligned into the Xenon light beam first. Since the Background doesn't take light in, it doesn't matter what is aligned when it is taken, but setting up the buffer first allows the Background and Reference to be taken one after the other.
3. Take Background	
4. Open Xenon Shutter	To take the reference, there must be light from the MAX-302 Xenon Light Source.
5. Take Reference	
6. Close Xenon Shutter	The shutter should be closed while the sample is being aligned (step 7).
7. Align Sample	
8. Open Xenon Shutter	There must be light to take the signal as well.
9. Take Signal	
10. Close Xenon Shutter	

Appendix I: Laser Program Parameters

Table I.1 Laser Program Parameters. A description of the important variables that can be set in the Andor Basic Laser program.

LaserIterations	Can be set to a value of 0, 1, or 2.
	0 - No laser iterations. Time Series Experiment.
	1 - Manual Laser iterations. Laser Iteration Experiment. When taking signal, the program will repeatedly take signal data as many times as the ok button is clicked.
	2 - Set Laser iterations. Laser Iteration Experiment. When taking signal, the program will repeatedly take signal data as many times as specified by Iteration Number.
IterationNumber	Specifies the number of signal spectra to take when LaserIterations is set to 2 (not used when LaserIterations is set to 0 or 1).
LITimePoint	The time point to use in Laser Iteration experiments. Time Series experiments have variable time points.
LaserWavelength\$	A string which is used to print the laser wavelength used in this experiment to the output log.
LaserEnergy\$	A string which is used to print the laser energy used in this experiment to the output log.
Temperature\$	A string which is used to print the temperature used in this experiment to the output log.
RootPath\$	file path string for the Main Folder where the data will be saved. This folder should contain subfolders for different Runs of the same type of experiment.
GateWidth	Gate Pulse Width in pico-seconds. Defines experimental time resolution. Should be of the same order as the desired timepoint.
AcquisitionMode	The desired Acquisition mode. [1-Single Scan; 2-Accumulate; 3-Kinetics]
AcquisitionNumber	The desired number of accumulations to use if AcquisitionMode is set to 2.
MCPGain	The desired MCPGain.
WavelengthCenter	The center point about which the range of the grating is centered. (Grating 1 is used for its larger range.)
NumberOfTimePoints	The number of timepoints to be collected in a Time Series Experiment.

RelaxationDelay\$	The amount of time (in seconds) after a time point that the relaxation period begins. LED illumination can happen during the relaxation period.
RelaxationTime\$	The duration of the relaxation period (in seconds).
FirstTimePoint	The first desired time point (in seconds).
LastTimePoint	The last desired time point (in seconds).
LogTime	The series of time points can be set as a logarithmic distribution of points or specific points set by the user.
	Setting LogTime to 0 has the program calculate the logarithmic time series.
	LogTime can be set to any other integer to define a time series. Below, an array is defined. The number of elements must match the value of NumberofTimePoints given above.

As an example, Table I.2 outlines some variables to be set for collecting a time series of a cyclic reaction of a light activated Photoactive Yellow Protein (PYP).

Table I.2 PYP Time Series Example Parameters. Example parameters for collecting a time series with 10 spectra averaged for each time point. The time series has 10 time points ranging from 1 microsecond to 1 second with a 4 second delay between each time point.

Variable	Value	Description
LaserIterations	0	Indicates that a time series will be taken.
AcquisitionMode	2	Accumulation averages the desired number of spectra together.
AccumulationNumber	10	The desired number of accumulations is 10.
WavelengthCenter	525	The center wavelength which covers the appropriate wavelength range for PYP is around 525 nm.
NumberofTimePoints	10	The desired number of time points is 10.
FirstTimePoint	0.000001	The first desired time point is 1 microsecond
LastTimePoint	1	The last desired time point is 1 second.
LogTime	0	Indicates that the desired number of time points will be spaced logarithmically.
RelaxationDelay\$	0.0	The relaxation time will begin immediately after each spectrum is taken.
RelaxationTime\$	4.0	The relaxation time will last for 4 seconds.

Appendix J: Hitfinder Code Listings

The Image constructor (Fig. J1) receives three arguments: an input file stream, a file name string, and a Boolean value. First, the constructor opens the stream and reads data from the given file (Fig. J2). Then, if the supplied Boolean value is true, the data is used to calculate the average pixel intensity (Fig. J3) and the upper outlier range value (Fig. J4). If the Boolean value is false, these are set to zero and can be calculated later. This functionality is important when reading many images in parallel as only one CPU core can read data from files into memory at a time. It is more efficient to have one core read in the data and let the rest of the cores do the calculations after the initial read.

```
Image::Image(std::ifstream &in, std::string name, bool full)
{
    in.open(name.c_str());
    Read(in, *this);
    filename = name;

    average = 0;
    thresh = 0;

    if (full)
    {
        Average(*this);
        Outlier(*this);
    }

    in.close();
}
```

Figure J.1 MarCCD Image Class Constructor. The constructor runs the Read, Average, and Outlier functions to create an object made up of information from the image.

```

std::ifstream &Read(std::ifstream &in, Image &image)
{
    unsigned short add;

    in.clear();
    in.seekg(1104, std::ios::cur);
    in.read((char*)&image.nfast, sizeof(image.nfast));
    in.read((char*)&image.nslow, sizeof(image.nslow));
    in.read((char*)&image.depth, sizeof(image.depth));

    in.seekg(552, std::ios::cur);
    in.read((char*)&image.beam_x, sizeof(image.beam_x));
    image.beam_x = (image.beam_x / 1000);
    in.read((char*)&image.beam_y, sizeof(image.beam_y));
    image.beam_y = (image.beam_y / 1000);

    in.seekg(44, std::ios::cur);
    in.read((char*)&image.xtal_to_detector, sizeof(image.xtal_to_detector));

    in.seekg(208, std::ios::cur);
    in.read((char*)&image.source_wavelength, sizeof(image.source_wavelength));

    in.seekg(4096, std::ios::beg);

    for (int i = 0; i < image.nslow; i++)
    {
        std::vector<unsigned short> new_row;
        image.data.push_back(new_row);

        for (int j = 0; j < image.nfast; j++)
        {
            in.read((char*)&add, sizeof(add));
            image.data[i].push_back(add);
        }
    }

    return in;
}

```

Figure J.2 MarCCD Image Class Read Function. The function reads in important values from the image header and uses them to read the image's pixel intensities into a two-dimensional array.

```

void Average(Image &image)
{
    unsigned long long Sum = 0;

    for (int i = 0; i < image.nslow; i++)
    {
        for (int j = 0; j < image.nfast; j++)
        {
            Sum += image.data[i][j];
        }
    }

    image.average = Sum / (image.nfast * image.nslow);
}

```

Figure J.3 MarCCD Image Class Average Function. The function takes the average of the image's pixel intensities.

```

void Outlier(Image &image)
{
    std::vector<unsigned short> Sorted;

    for (int i = 0; i < image.nslow; i++)
    {
        for (int j = 0; j < image.nfast; j++)
        {
            if (image.data[i][j] > image.average)
            {
                Sorted.push_back(image.data[i][j]);
            }
        }
    }

    std::sort(Sorted.begin(), Sorted.end());
    double q1, q3;

    if (Sorted.size() % 4 == 1)
    {
        int n = (Sorted.size() - 1) / 4;
        q1 = (double)((0.25 * Sorted[n]) + (0.75 * Sorted[n + 1]));
        q3 = (double)((0.75 * Sorted[(3 * n) + 1]) + (0.25 * Sorted[(3 * n) + 2]));
    }
    else if (Sorted.size() % 4 == 3)
    {
        int n = (Sorted.size() - 3) / 4;
        q1 = (double)((0.75 * Sorted[n + 1]) + (0.25 * Sorted[n + 2]));
        q3 = (double)((0.25 * Sorted[(3 * n) + 2]) + (0.75 * Sorted[(3 * n) + 3]));
    }
    else
    {
        int n = (Sorted.size() / 2);
        std::vector<unsigned short> lower = std::vector<unsigned short>
range(&Sorted[0], &Sorted[0] + n);
        std::vector<unsigned short> upper = std::vector<unsigned short>
range(&Sorted[n], &Sorted[n] + n);

        if (n % 2 == 0)
        {
            int m = n / 2;
            q1 = (double)(lower[m - 1] + lower[m]) / 2;
            q3 = (double)(upper[m - 1] + upper[m]) / 2;
        }
        else
        {
            int m = (n - 1) / 2;
            q1 = (double)lower[m];
            q3 = (double)upper[m];
        }
    }

    double IQR = (q_3 - q_1);
    image.thresh = (q_3 + (3.0 * IQR));
}

```

Figure J.4 MarCCD Image Class Outlier Function. The function calculates the Interquartile Range of the pixel intensities in the dataset that are above the average and uses it to calculate the lower threshold of what is considered an outlier.

```

omp_set_num_threads(args.core_num);
#pragma omp parallel shared(images, hit_list) private(thread_id, spots) {
    #pragma omp single {
        args.core_num = omp_get_num_threads();
        done.resize(args.core_num, 0);

        Image Add(input, filenames[0], false);
        images.push_back(Add);
        while (images.size() < args.core_num) {
            Image Add(input, filenames[images_read], false);
            images.push_back(Add);
            images_read++;
        }
    }

    thread_id = omp_get_thread_num();
    if (thread_id == 0) {
        int next = 1;
        while (images_read < image_total) {
            if (done[next]) {
                Image Add(input, filenames[images_read], false);
                images[next] = Add;

                #pragma omp atomic
                done[next]--;

                images_read++;
                #pragma omp flush (images_read)
            }
            next = (next % (args.core_num - 1)) + 1;
        }
    }
    else {
        while (true) {
            if (done[thread_id] == 0) {
                Average(images[thread_id]);
                Outlier(images[thread_id]);
                spots = Spot_Count(images[thread_id], args.spot_size);

                if (spots > args.spot_num) {
                    addf = images[thread_id].get_filename();
                    hit_list.push_back(addf);
                }

                time(&t3);
                if (args.gui_flag == true && thread_id == 1) {
                    sec = difftime(t3, t1);
                    std::cout << "Status:" << images_read << ":" << hit_list.size()
<< ":" << image_total << ":" << sec << std::endl;
                }

                #pragma omp atomic
                done[thread_id]++;
            }

            #pragma omp flush (images_read)
            if (done[thread_id] == 1 && images_read == image_total) { break; }
        }
    }
}
#pragma omp barrier

```

Figure J.5 Hitfinder Program Main Function Parallel Loop. The parallel loop opens the requested number of threads and has one read in images while the rest check the rest for diffraction. Images which are determined to contain diffraction are added to the hitlist file. Status information is sent to the standard output stream.

```

int Spot_Count(Image &image, int spot_size)
{
    int count = 0;
    int sub_count = 0;
    int area = 0;
    unsigned int &height = image.get_height();
    unsigned int &width = image.get_width();
    double &thresh = image.get_threshold();
    Image::usrt_vec_2d &data = image.get_data();

    for (int i = 1; i < (height - 1); i++)
    {
        for (int j = 1; j < (width - 1); j++)
        {
            if(data[i][j] > thresh)
            {
                for (int k = (-1 * spot_size); k <= spot_size; k++)
                {
                    for (int l = (-1 * spot_size); l <= spot_size; l++)
                    {
                        area++;
                        if ((data[i + k][j + l] > thresh) && (data[i + k][j + l] <= data[i][j]))
                        {
                            sub_count++;
                        }
                    }
                }

                if (sub_count == area)
                {
                    count++;
                }

                sub_count = 0;
                area = 0;
            }
        }
    }

    return count;
}

```

Figure J.6 Hitfinder Program Spot Count Function. The function checks the pixels around each pixel which is above the threshold to make sure that they are also above the threshold.